6. Formulation, development and evaluation of CS encapsulated solid lipid nanoparticles (CS-SLNs)

6.1 Experimental methods

6.1.1 Pre-formulation studies

Preformulation study is the first step in rational development of dosage form of any drug molecule [175]. Hence, the following preformulation studies were performed for successful development of CS-SLNs.

6.1.1.1 Drug excipients compatibility studies

6.1.1.1.1 Fourier transform infrared (FTIR) spectroscopy

FTIR spectroscopic study of CS, Glyceryl monostearate (GMS), PVA and their physical mixture was conducted using FTIR spectrophotometer (Shimadzu, Model-8400S, Japan) in order to assess the possibility of chemical interaction, if any, between CS and other excipients. The analysis was performed by following the same protocol as mentioned in ***sub-section 5.1.1.2.1.***

6.1.1.1.2 Differential scanning calorimetry (DSC) study

The thermal behaviour of CS, GMS, PVA and their physical mixture was characterized by using TGA/DSC-1, Star® system (Mettler Toledo, Switzerland) with an auto cool accessory, for evaluating the compatibility of CS with other excipients. The analysis was performed by following the same protocol as mentioned in ***sub-section 5.1.1.2.2.***

6.1.2 Formulation of CS encapsulated solid lipid nanoparticles

CS-SLNs were prepared based on double emulsification solvent evaporation ($W_1/O/W_2$) method with suitable modifications [29]. Briefly, 0.5 ml of aqueous phase

containing 25 mg of CS (W_1; internal aqueous phase) was emulsified with the weighed amount of GMS and Span 80 containing dichloromethane (DCM) (O; organic phase), with the help of ultra probe sonicator (UP50H, Hielscher, USA) for 90 sec at 80% sonication amplitude. This obtained primary emulsion (W_1/O) was poured into external aqueous phase (W_2), containing PVA and 0.1 % v/v acetic acid under constant stirring. Then, the whole mixture was sonicated under ice bath using ultra probe sonicator for 5 min at 80% sonication amplitude. The resultant double emulsion (W_1/O/W_2) was allowed to stirr magnetically at 1000 rpm for 24 hr at room temperature in order to evaporate residual DCM completely and to form CS-SLNs. Subsequently, the resulting CS-SLNs were centrifuged at 15,000 rpm for 15 min at 4 ^{o}C temperature, using cooling centrifuge (RC 4100 F, Eltek, Mumbai, India). The supernatant was kept for drug content analysis as described later and sediment was washed thrice with DDW. CS-SLNs were resuspended in DDW containing 2 % (w/v) mannitol as cryoprotectant and finally lyophilized using freeze drier (Labconco, USA) for 48 hr, at -45 ^{o}C with a vacuum pressure of 0.050 mbar. The lyophilized CS-SLNs were stored in a desiccator at 4 ^{o}C until further use [49].

6.1.3 Experimental design

6.1.3.1 Preliminary screening of variables by using Plackett-Burman screening design

A set of experiments with Plackett–Burman statistical experimental design was performed to screen the effect of various formulation and process variables on the CQAs of CS-SLNs as described in ***sub-section 5.1.3.1***. The Design Expert® software (Version 8.0.6.1, Stat-Ease Inc., Minneapolis, USA) was utilized for the generation of randomized design matrix and evaluation of statistical experimental design. Each

variable was represented at two levels, namely, "high" and "low". These levels define the upper and lower limits of the range covered by each variable. The level selection of different variables was based on a preliminary study and findings in the existing scientific literature. Different 11 independent variables were tested using 12 experimental runs. The selected experimental variables along with their levels, used for the screening design are depicted in Table 6.1.

Table 6.1 Experimental variables with their levels in Plackett-Burman screening design

Variables	**Level**	
Independent Variables	Low (-1)	High (+1)
A : Concentration of lipid (%w/v)	0.3	1
B : Concentration of external surfactant (%w/v)	0.5	1.5
C : Organic phase/aqueous phase ratio	0.17	0.33
D : Stirring speed (rpm)	1000	1500
E : Sonication time (min)	3	6
F : Sonication amplitude (%)	40	80
G : Types of organic phase	DCM	CLF
H : Concentration of internal surfactant (%w/v)	0.05	0.1
I : Types of drug	CS	GAN
J : Ratio of organic phase (DCM/CLF)	3:2	4:1
K : Stirring temp (^{o}C)	25	40

Where, DCM: Dichloromethane; CLF: Chloroform; CS: Cromolyn sodium; GAN: Ganciclovir

The particle size (Y_1), EE (Y_2) and PDI (Y_3) of CS-SLNs were selected as dependent variables (CQAs). Results of the different experimental runs were analyzed by employing multiple linear regressions using one-way ANOVA, in order to determine

the significance of the selected model along with the factor coefficients. Results obtained were statistically analyzed at 5 % level of significance. All experiments were performed in a triplicate and randomized order [54, 177, 178].

6.1.3.2 Optimization of variables by using Box-Behnken Experimental Design

The critical variables obtained after preliminary screening through the Plackett-Burman screening design, were applied to RSM for statistical optimization of the CS-SLNs. In current study, a response surface method, 3-level, 3-factor, Box-Behnken experimental design with statistical model incorporating interactive and polynomial terms was utilised for optimization, quantification and establishing the relationship between the clusters of controlled independent variables and the physicochemical properties of CS-SLNs [179-182], as described in ***sub-section 5.1.3.2***.

Based on initial screening in the preliminary studies, concentration of lipid (X_1), concentration of surfactant (X_2) and organic phase/aqueous phase ratio (X_3) were opted as three critical independent variables. Each critically selected variable is varied at three different levels. Higher, middle and lower level of each variable is coded as +1, 0 and -1, respectively. Other variables, which were evaluated in the preliminary Plackett-Burman screening design, were adjusted to the fixed level in the Box-Behnken experimental design owing to their statistically insignificant effects on the dependent variables. The studied particle size (Y_1), EE (Y_2) and PDI (Y_3) of prepared CS-SLNs were taken as dependent variables. All independent and dependent variables along with applied constraints, in the form of actual and coded levels are summarized in Table 6.2. The design matrix comprising of 17 runs, along with quadratic response surface and second order polynomial model was constructed by using Design-Expert software® (8.0.6.1, Stat-Ease Inc., Minneapolis, USA). The possible source of

experimental bias and variability was deflected by randomizing the order of experimental run.

Multiple linear regression was applied by employing the ANOVA, in order to ascertain the influence and significance of factors along with their interactive effect on the response variables. Numerical output of ANOVA was represented in terms of *p*-value and $p<0.05$ was considered as statistically significant. 3D response surface plots and second order polynomial models were generated to quantify the correlation between independent variables and dependent variables as well as to determine design space [179, 181]. Further, desirability approach based numerical optimization technique was probed by fixing the different constraints in order to obtain the levels of independent variables, which would yield optimized CS-SLNs with desired quality traits [49, 179, 183]. The optimized CS-SLNs were further utilized for various characterizations, *in-vitro* and *in-vivo* evaluation studies.

Table 6.2 Independent variables with their levels and dependent variables in Box-Behnken experimental design

Independent variables	**Coded levels of variables**		
	Low	**Medium**	**High**
	-1	0	1
X_1 = Concentration of lipid (%w/v)	0.3	0.65	1
X_2 = Concentration of surfactant (%w/v)	0.5	1	1.5
X_3 = Organic phase/aqueous phase ratio (v/v)	0.17	0.25	0.33
Dependent variables (Responses)	**Constraints**		
Y_1= Particle size (nm)	Minimize		
Y_2= Encapsulation efficiency (%)	Maximize		
Y_3= Polydispersity index (PDI)	Minimize		

6.1.4 Characterizations of CS-SLNs

6.1.4.1 Particle size, polydispersity index (PDI) and zeta potential

Measurement of particle size, zeta potential and PDI of prepared CS-SLNs was carried out using photon correlation spectroscopy using DELSA^{TM} NANO C particle size analyzer (Beckman Coulter, Inc., UK) at 25 ^{o}C temperature by following the same protocol as mentioned in the ***sub-section 5.1.4.1***. All measurements were performed in the triplicates and mean value considered for the analysis of data.

6.1.4.2. Encapsulation efficiency (EE) and drug loading

The EE (%) and drug loading (%) of prepared CS-SLNs were determined indirectly by following the same estimation protocol and same instrument as mentioned in the ***sub-section 5.1.4.2.***

6.1.4.3 Solid state characterizations

6.1.4.3.1 Fourier transform infrared spectroscopy (FTIR) study

The FTIR spectra of pure CS, GMS, PVA and optimized CS-SLNs were recorded by following the same protocol and same instrument as mentioned in the ***sub-section 5.1.1.2.1*** in order to evaluate any significant change, if occurs, during the encapsulation of CS inside the solid lipid nanoparticles (SLNs). The scanning was performed over the wavenumber ranging from 4000 to 400 cm^{-1} at room temperature and the resolution was set at 4 cm^{-1}.

5.1.4.3.2 Differential scanning calorimetry (DSC) study

The physical state of CS inside SLNs was assessed by DSC study. The thermograms of pure CS, GMS, PVA and optimized CS-SLNs were recorded by following the same protocol and same instrument as mentioned in the ***sub-section 5.1.1.2.2***.

6.1.4.3.3 Powder X-ray diffractometry (PXRD) study

The PXRD patterns of pure CS, GMS, PVA, physical mixture and optimized CS-SLNs were obtained by following the same protocol and same instrument as mentioned in the ***sub-section 5.1.4.3.3.***

6.1.4.4 Shape and surface morphology

6.1.4.4.1 High resolution transmission electron microscopy (HR-TEM)

The shape and surface morphology of the optimized CS-SLNs was examined by following the same protocol and same instrument as mentioned in the ***sub-section 5.1.4.4.1.***

6.1.4.4.2 Atomic force microscopy (AFM)

The surface morphology of optimized CS-SLNs was visualized by following the same protocol and same instrument as mentioned in the ***sub-section 5.1.4.4.2.***

6.1.4.5 *In-vitro* drug release study

The *in-vitro* drug release study of optimized CS-SLNs was performed using modified dialysis bag diffusion technique in phosphate buffer pH 7.4. The same protocol was followed for *in-vitro* drug release study and release kinetic modeling as mentioned in the ***sub-section 5.1.4.5.***

6.1.4.6 Accelerated and real time storage stability study

The stability of optimized CS-SLNs was assessed over a period of 6 month at room temperature (25 $\pm$ 2 ^{o}C), refrigerated condition (4 $\pm$ 1 ^{o}C), and accelerated condition (40 $\pm$ 2 ^{o}C/75 $\pm$ 5 % RH) as per ICH guideline by following the same protocol as mentioned in the ***sub-section 5.1.4.6.***

6.1.4.7 Animal studies

6.1.4.7.1 Animals

The animal study protocol was duly approved by Central Animal Ethical Committee of Banaras Hindu University (No. Dean/2014/CAEC/856). The animal details are discussed earlier in ***sub-section 5.1.4.7.1.***

6.1.4.7.2 *Ex-vivo* intestinal permeation study

The intestinal permeation potential of CS-SLNs across the GIT was assessed by *ex-vivo* intestinal permeation study using non-everted gut sac technique by following the same method as described in **s*ub-section 5.1.4.7.2.***

6.1.4.7.3 *In-vivo* intestinal uptake study

The intestinal particulate uptake and permeation of CS-SLNs was visualized by CLSM upon oral administration of coumarin-6 loaded CS-SLNs in rats. *In-vivo* intestinal uptake study was performed by following the same method as described in **s*ub-section 5.1.4.7.3.***

6.1.4.7.4 *In-vivo* pharmacokinetic study

6.1.4.7.4.1 *Dosing and sampling*

The same dosing and sampling protocol as described in **s*ub-section 5.1.4.7.4.1*** was followed for the determination of pharmacokinetic profile of CS-SLNs after oral administration in the rats.

6.1.4.7.4.2 *Chromatography conditions and drug extraction*

The same in-house validated RP-HPLC method was followed for determination of CS concentration in blood plasma as described in ***sub-section 4.1.2*.** The details of

chromatography conditions and drug extraction are mentioned in ***sub-section 4.1.2.1 and 4.1.2.4***, respectively.

6.1.4.7.4.3 *Pharmacokinetic parameters*

Various pharmacokinetic parameters for CS-SLNs were determined as mentioned in ***sub-section 5.1.4.7.4.3*** using non-compartmental analysis of plasma drug concentration-time profile data through Winnonlin® 6.1 (Pharsight Corporation, Mountain View, CA) pharmacokinetic software.

6.1.4.7.5 *In-vivo* mast cell stabilizing activity

In-vivo mast cell stabilizing activity was studied by following the same protocol as mentioned in ***sub-section 5.1.4.7.5*** after oral administration of CS-SLNs in rats.

6.1.4.8 Statistical analysis

The similar statistical analysis was performed using the GraphPad Prism software (version 5.03, GraphPad Software, USA) as mentioned in ***sub-section 6.1.4.8.***

6.2 Results and discussions

6.2.1 Pre-formulation studies

6.2.1.1 Drug excipients compatibility studies

6.2.1.1.1 Fourier transform infrared (FTIR) spectroscopy

FTIR study was performed with an objective to evaluate the compatibility of CS with other excipients, which would be used for the preparation of CS-SLNs. The FTIR spectra of CS, GMS, PVA and their physical mixture are shown in Figure 6.1. FTIR spectra of CS (Figure 6.1 (a)) exhibited the characteristic basic peaks corresponding to C=O (1639.54 cm^{-1}), asymmetric COO^- (1573 cm^{-1}), symmetric COO^- (1410 cm^{-1}), O-H (3416 cm^{-1}), C-H alkane (2880 cm^{-1}) and aromatic C-H (1477 cm^{-1}). In

additions, large number of characteristic bands was also observed across the fingerprint region (1400–600 cm^{-1}) due to vibration within the molecule [43, 45, 49]. The characteristic bands of GMS were attributed to C-H stretching (2840-2960 cm^{-1}), C-H bending (850-700 cm^{-1}) and C=O stretching (1730 cm^{-1}) as depicted in Figure 6.1 (b) [237]. FTIR spectra of PVA (Figure 6.1 (c)) showed all the major peaks, including C-H stretching (2840-3000 cm^{-1}) from alkyl group and O-H stretching from the hydrogen bonds (intermolecular and intramolecular) (3200-3550 cm^{-1}). It also depicted the peaks related to C=O stretching together with C-O stretching from the acetate group (1750-1735 cm^{-1}) [206].

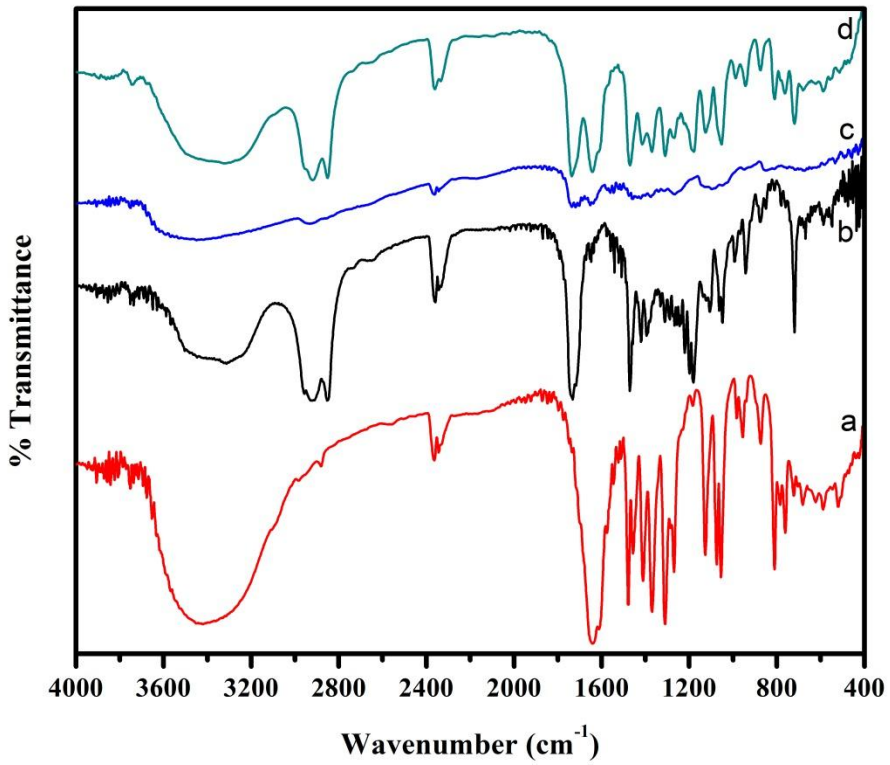

Figure 6.1 FTIR spectra of (a) CS, (b) GMS, (c) PVA and (d) physical mixture

All the major peaks related to CS, GMS and PVA were retained in FTIR spectra of the physical mixture (Figure 6.1 (d)) at nearly same wavenumber, indicating an

absence of any interaction of CS with other excipients and existence of compatibility with each other [40, 49].

6.2.1.1.2 Differential scanning calorimetry (DSC) study

DSC thermograms of CS, GMS, PVA and their physical mixture are depicted in Figure 6.2. The DSC thermogram of pure CS (Figure 6.2 (a)) showed characteristic endothermic peak at 264 ^{o}C corresponding to its melting point, indicating its crystalline nature [149]. GMS and PVA showed sharp endotherm at 62 ^{o}C and 226 ^{o}C corresponding to their respective melting points (Figure 6.2 (b) & (c)).

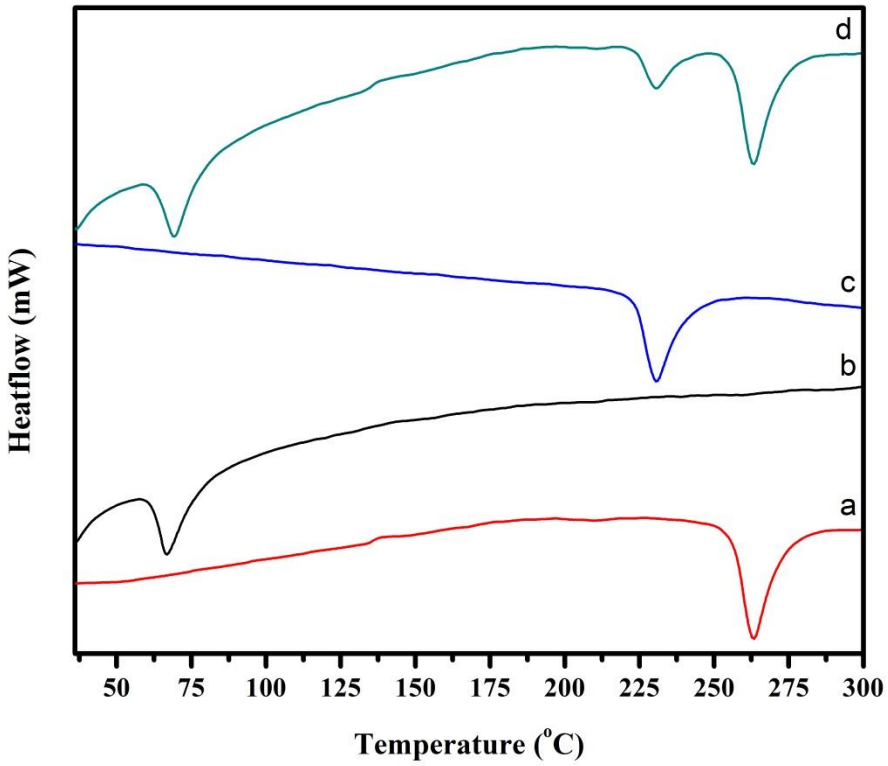

Figure 6.2 DSC thermograms of (a) CS, (b) GMS, (c) PVA and (d) physical mixture

The physical mixture of CS along with GMS and PVA showed nearly same thermal behaviour as the individual components without any considerable shift of endothermic

peak (Figure 6.2 (d)), suggesting the absence of interaction of CS and excipients with each other. Moreover, no any new endothermic or degradation peak was observed in the thermogram of physical mixture, suggesting the existence of compatibility between CS and other excipients, which would be used for the preparation of CS-SLNs [45, 49, 207].

6.2.2 Experimental design

6.2.2.1 Preliminary screening of variables by using Plackett-Burman screening design

The physicochemical properties of CS-SLNs prepared by double emulsification solvent evaporation ($W_1/O/W_2$) method are influenced by various formulation and process variables. The influence of various independent variables on the dependent variables, i.e., particle size, EE and PDI of the CS-SLNs (CQAs) were studied by 11-factor, 2-level Plackett-Burman screening design. The Plackett–Burman statistical experimental design was employed for the initial screening and selection of critical variables affecting significantly to the formulation characteristics of CS-SLNs, with good degree of accuracy during preliminary studies [208, 209]. Based on literature search and existing scientific knowledge, various independent variables were selected as they are likely to affects the physicochemical properties of CS-SLNs. A total of 12 experimental trials, comprising of various combinations of different 11 independent variables were carried out as shown in Table 6.3. Since Plackett-Burman screening designs are resolution 4 designs, only main effects of the selected independent variables were analyzed. The wide variation was observed in the selected dependent variables of CS-SLNs, suggesting that the independent variables had a significant effect on the response parameters chosen. Table 6.4 shows the results of different

experimental runs in terms of different dependent variables. Pareto chart showing the relative effect of the each independent variable on each dependent variable is depicted in Figure 6.3. It indicates the effect of independent variables plotted against the vertical axis as per their respective rank order. The variables for which vertical bars extending passed the horizontal line suggested the statistical significance on the dependent variable [210].

Table 6.3 Plackett-Burman screening design experimental matrix

Run	A	B	C	D	E	F	G	H	I	J	K
1	1.00	1.50	0.33	1000	3	40	CLF	0.05	GAN	4:1	25
2	0.3	1.50	0.17	1500	6	40	CLF	0.1	GAN	3:2	25
3	0.3	1.50	0.33	1000	6	80	CLF	0.05	SCG	3:2	40
4	0.3	0.50	0.17	1000	3	40	DCM	0.05	SCG	3:2	25
5	0.3	1.50	0.33	1500	3	40	DCM	0.1	SCG	4:1	40
6	1.00	0.50	0.33	1500	3	80	CLF	0.1	SCG	3:2	25
7	1.00	1.50	0.17	1000	3	80	DCM	0.1	GAN	3:2	40
8	0.3	0.50	0.33	1000	6	80	DCM	0.1	GAN	4:1	25
9	1.00	1.50	0.17	1500	6	80	DCM	0.05	SCG	4:1	25
10	0.3	0.50	0.17	1500	3	80	CLF	0.05	GAN	4:1	40
11	1.00	0.50	0.17	1000	6	40	CLF	0.1	SCG	4:1	40
12	1.00	0.50	0.33	1500	6	40	DCM	0.05	GAN	4:1	40

Where, DCM: Dichloromethane; CLF: Chloroform; CS: Cromolyn sodium; GAN: Ganciclovir

Table 6.4 Results of dependent variables obtained through Plackett-Burman design

Run	Particle Size (nm)	EE (%)	PDI
1	703 ± 2.8	24 ± 1.1	0.297 ± 0.026
2	582.6 ± 2.1	16.1 ± 0.5	0.198 ± 0.017
3	541.2 ± 3.4	13.7 ± 1.9	0.17 ± 0.029
4	745.8 ± 5.8	30.1 ± 0.9	0.389 ± 0.048
5	484 ± 1.1	11.8 ± 2.7	0.13 ± 0.094
6	760.2 ± 1.8	33.4 ± 0.3	0.412 ± 0.037
7	697.4 ± 3.9	22.4 ± 0.7	0.278 ± 0.024
8	673.1 ± 4.2	19.8 ± 1.4	0.247 ± 0.065
9	673 ± 0.8	19.3 ± 1.1	0.218 ± 0.012
10	726 ± 5.1	26.3 ± 1.5	0.321 ± 0.074
11	779.5 ± 2.3	35.6 ± 1.7	0.432 ± 0.026
12	738 ± 4.8	28.1 ± 0.3	0.362 ± 0.032

All values reported are mean ± SD; n = 3

Statistical analysis revealed that the particle size (Y_1) of the CS-SLNs was significantly (p<0.05) influenced by four independent variables, i.e., concentration of lipid (A), concentration of surfactant (B), organic phase/aqueous phase ratio (C) and stirring speed (D), as indicated in Figure 6.3 (A) and Table 6.5. The value of correlation coefficient (R^2) was found to be 0.9922, indicating the goodness of fit of the model being tested. The p-value for the regression model was found to be 0.0044 and was considered as significant. All other independent variables showed non-significant (p>0.05) impact on the particle size. The model fitting values for different dependent variables, which indicate model adequacy are listed in Table 6.6.

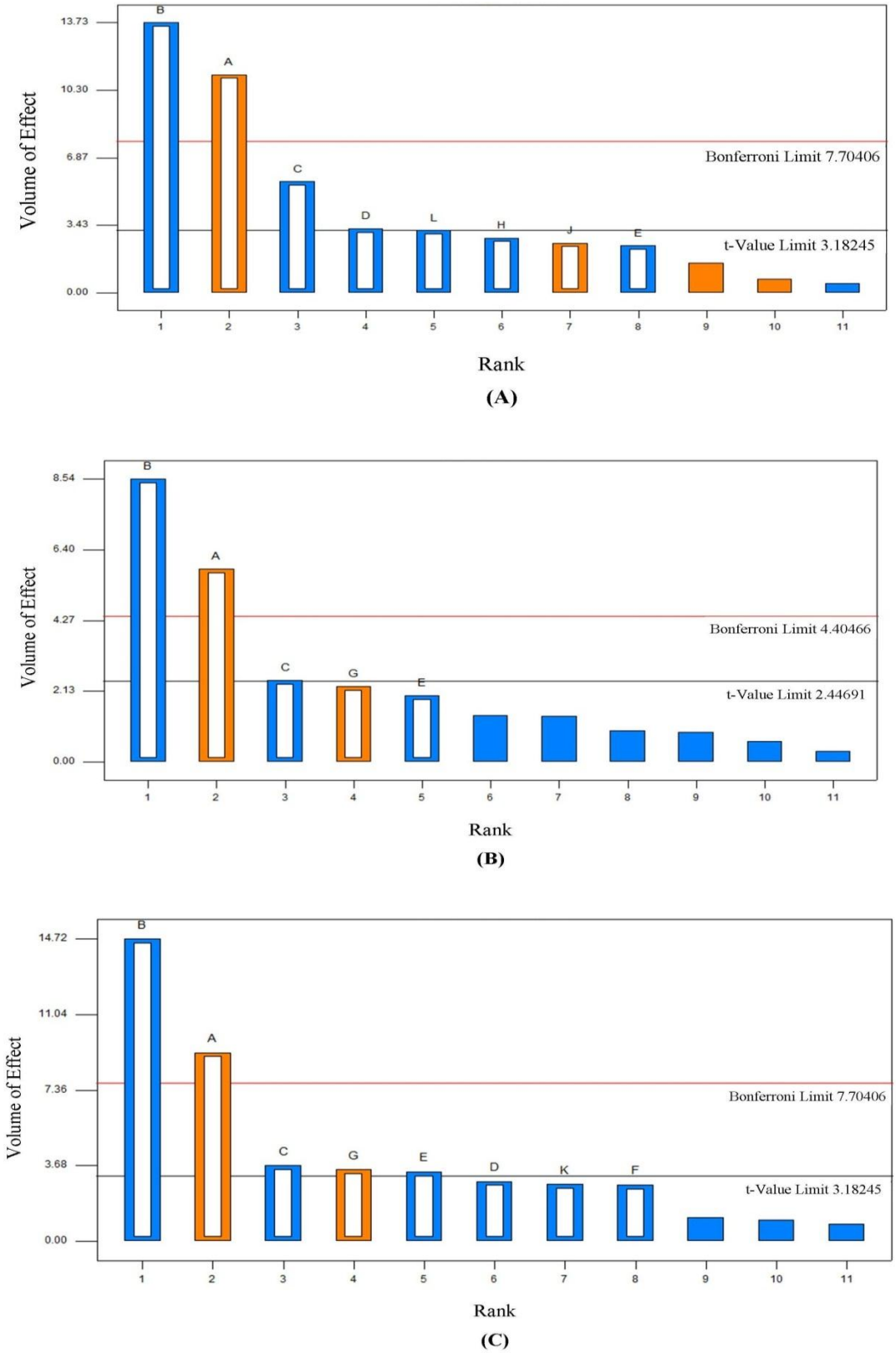

Figure 6.3 Pareto charts showing the significant effect of independent variables on (A) particle size, (B) EE and (C) PDI of CS-SLNs during Plackett-Burman screening design

Table 6.5 Statistical analysis of dependent variables of Plackett-Burman screening design

Factor	Y_1 = Particle size		Y_2 = EE		Y_3 = PDI	
	Coefficient	***p* Value**	**Coefficient**	***p* Value**	**Coefficient**	***p* Value**
A	49.87	0.0016	3.75	0.0011	0.045	0.0027
B	-61.78	0.0008	-5.50	0.0001	-0.073	0.0007
C	-25.40	0.0110	-1.58	0.0493	-0.018	0.0348
D	-14.68	0.0470	-0.88	0.1361	-0.014	0.0623
E	-10.75	0.0968	-1.28	0.0935	-0.017	0.0432
F	3.17	0.3888	-0.90	0.1813	-0.013	0.0717
G	6.77	0.1317	1.47	0.0631	0.017	0.0401
H	-12.52	0.0689	-0.20	0.1000	-0.005	0.4296
I	11.37	0.0857	-0.60	0.2523	-0.004	0.1000
J	-2.22	0.1000	-0.58	0.2064	-0.014	0.0697
K	-14.30	0.0502	-0.40	0.2952	-0.005	0.3373

For EE (Y_2) of the CS-SLNs, the three most significant ($p<0.05$) independent variables were concentration of lipid (A), concentration of surfactant (B) and organic phase/aqueous phase ratio (C) amongst all other independent variables selected, as depicted in Figure 6.3 (B) and Table 6.5. The R^2 value for the regression model was 0.9531, indicating the goodness of fit of the model being tested. The *p*-value for the regression model was found to be significant ($p=0.0006$), confirming the adequate fitting to the model. All other independent variables also affected EE but their impact was statistically non-significant ($p>0.05$).

Table 6.6 Model summary statistics of the quadratic response surface models

Response Variable	Model						
	F-value	**Prob>F***	**R^2**	**Adj. R^2**	**Pred. R^2**	**Adeq. Prec.**	**C.V. (%)**
Y_1	47.98	0.0044	0.9922	0.9716	0.8759	20.890	2.31
Y_2	24.39	0.0006	0.9531	0.9140	0.8124	13.962	9.54
Y_3	45.20	0.0048	0.9918	0.9698	0.8684	20.392	5.94

*Adj. R^2: Adjusted R^2; Pred. R^2: Predicted R^2; Adeq. Prec.: Adequate Precision; C.V.: Coefficient of Variation; *Prob>F is the significance level and a value less than 0.05 considered significant.*

Whereas, PDI of the CS-SLNs was found to be most significantly (p<0.05) dependent on the concentration of lipid (A), concentration of surfactant (B) and organic phase/aqueous phase ratio (C), sonication time (E) and types of organic phase (G) relative to other variables, as observed in Figure 6.3 (C) and Table 6.5. The R^2 value for the regression model was found to be 0.9918, suggesting the significant goodness of fit of the model. The significant p-value (p=0.0048) for the regression model confirmed the adequate fitting to the model. All other independent variables showed non-significant (p>0.05) impact on the PDI. Thus, on the basis of results of the Plackett–Burman screening design, all the significantly affected independent variables on the physicochemical properties of CS-SLNs were further evaluated by RSM for statistical optimization [54, 209, 210].

6.2.2.2 Formulation optimization of variables by using Box-Behnken experimental design

According to the results obtained from the Plackett-Burman screening design, the total of three common independent variables, namely concentration of lipid, concentration of surfactant and organic phase/aqueous phase ratio were selected as

critical variables for the statistical optimization of the CS-SLNs using RSM. Whereas, other independent variables, which have affected significantly on the single dependent variables, were fixed to their higher or lower level corresponding to their negative or positive effect, respectively [49, 209, 210]. A 3-level, 3-factor Box-Behnken experimental design based RSM was performed for precisely exploring and optimizing the influence of three independent variables i.e. concentration of lipid (X_1), concentration of surfactant (X_2) and organic phase/aqueous phase ratio (X_3) on dependent variables such as particle size (Y_1), EE (Y_2) and PDI (Y_3) of CS-SLNs. A total of 17 batches of CS-SLNs including 5 center points, were prepared as per design matrix generated by Box-Behnken experimental design by varying the three independent variables for all possible combinations. All the other independent variables used in the Plackett-Burman screening design, were found to have statistically non-significant effect on the physicochemical properties of CS-SLNs in the selected range and hence, set to fix level during optimization using RSM [209, 210]. The statistical treatment combinations of the different independent variables along with the measured response variables obtained by performing experiments are summarized in Table 6.7.

Regression models and polynomial equations explaining the main effect, interactive effect as well as quadratic effect of the various independent variables on dependent variables were generated by fitting the results of the experimental design with the help of Design-Expert® software. Statistical significance of the selected model and the regression coefficients were estimated by multiple regressions using ANOVA. For each response, the model which generated a higher F value was selected as the best fitted model. The accuracy and adequacy of the model was determined by measuring

the R^2 value, which indicates the 'goodness of fit' of the model to the experimental results.

Table 6.7 Box-Behnken experimental design showing experimental runs with independent variables and their measured responses: particle size (Y_1), encapsulation efficiency (Y_2), and PDI (Y_3) of CS-SLNs

Run No.	Independent variables			Dependent variables		
	X_1	X_2	X_3	Y_1	Y_2	Y_3
Factorial Points						
1	-1	-1	0	489.2 ± 2.7	31.8 ± 1.3	0.289 ± 0.02
2	1	-1	0	561.4 ± 1.4	35.2 ± 2.4	0.386 ± 0.035
3	-1	1	0	387.1 ± 5.7	15.2 ± 1.1	0.138 ± 0.1
4	1	1	0	499.3 ± 6.1	32.1 ± 0.7	0.304 ± 0.078
5	-1	0	-1	431.7 ± 9.2	22.1 ± 2.6	0.229 ± 0.1
6	1	0	-1	539.2 ± 13.4	33.8 ± 3.9	0.372 ± 0.046
7	-1	0	1	399.3 ± 3.4	17.4 ± 1.6	0.161 ± 0.12
8	1	0	1	463.3 ± 6.1	29.1 ± 0.3	0.251 ± 0.23
9	0	-1	-1	517.8 ± 7.3	32.2± 0.5	0.348 ± 0.07
10	0	1	-1	418 ± 8.2	20.1 ± 1.2	0.194 ± 0.034
11	0	-1	1	447.4 ± 2.4	24.9 ± 2.1	0.245± 0.086
12	0	1	1	370.2 ± 2.9	12.5 ± 1.9	0.116 ± 0.042
Centre Points						
13	0	0	0	470.3 ± 3.8	31.2± 0.6	0.240 ± 0.078
14	0	0	0	482 ± 7.4	31.0 ± 1.4	0.251 ± 0.091
15	0	0	0	477.8 ± 4.8	30.4 ± 0.7	0.243 ± 0.042
16	0	0	0	485.1 ± 5.9	31.7 ± 0.9	0.239 ± 0.012
17	0	0	0	488.2 ± 12.4	29.6 ± 1.8	0.247 ± 0.067

All data are shown as mean ±S.D; n=3.

The positive coefficient in polynomial equation suggests that the response varies directly with successive increase in the value of independent variables (i.e.,

synergistic effect), whereas the negative sign indicates that the response decreases with successive increase the value of independent variables (i.e., inverse effect). The absolute value of the co-efficient indicates the magnitude of effect of the independent variables on the response variable; the higher the value the higher the magnitude [179, 211-213].

Table 6.8 Statistical analysis of dependent variables of Box-Behnken experimental design along with estimated regression coefficients and associated *p* values

Factor	Y_1 = Particle size		Y_2 = EE		Y_3 = PDI	
	Coefficient	***p* Value**	**Coefficient**	***p* Value**	**Coefficient**	***p* Value**
Intercept	480.68	< 0.0001	30.78	< 0.0001	0.24	< 0.0001
X_1	44.49	< 0.0001	5.46	< 0.0001	0.062	< 0.0001
X_2	-42.65	< 0.0001	-5.53	< 0.0001	-0.064	< 0.0001
X_3	-28.31	< 0.0001	-3.04	0.0002	-0.046	< 0.0001
X_1X_2	10.00	0.0120	3.38	0.0009	0.017	0.0055
X_1X_3	-10.88	0.0081	0.000	1.0000	-0.013	0.0189
X_2X_3	5.65	0.0991	-0.075	0.9058	0.0062	0.1951
X_1^2	11.80	0.0047	0.48	0.4426	0.031	0.0002
X_2^2	-8.23	0.0251	-2.69	0.0028	0.0038	0.3925
X_3^2	34.10	< 0.0001	-5.66	< 0.0001	-0.022	0.0012

3D response surface plots were constructed using respective polynomial equations to reveal the interactive effect of any two independent variables on dependent variable graphically, keeping third one at a constant level. The relationships between the dependent variable and the independent variables were also visualized by 2D contour plots for understanding the relative influence of the independent variable along with

in combinations [179, 180, 182]. The mathematical relationships of independent variables' coefficients along with corresponding *p*-values for the dependent variables obtained by regression analysis are summarized in Table 6.8. *p*-value less than 0.05 was considered as statistically significance.

6.2.2.2.1 Influence of Independent variables on particle size

The particle size of prepared CS-SLNs was varied in the range from 370.2 $\pm$ 2.9 nm to 561.4 $\pm$ 1.4 nm as a consequence of the change in formulation variables in their limits. The quadratic model was selected for the statistical analysis of influence of independent variables on particle size based on the lack of fit test as shown in Table 6.9. The second-order mathematical polynomial equation with constant and regression coefficients, describing an empirical relationship between particle size (Y_1) and independent variables, generated by multiple linear regressions can be given as follows in terms of coded variables Eq (6.1):

$$Y_1 = 480.68 + 44.49X_1 - 42.65X_2 - 28.31X_3 + 10.0X_1X_2 - 10.88X_1X_3 + 11.80X_1^2 - 8.23X_2^2 - 34.10X_3^2 \quad \text{Eq (6.1)}$$

Non-significant lack of fit value (p=0.7810; p>0.05) with F-value of 0.37 indicated that quadratic model is best fit to the independent variables for significantly describing the effect on the particle size. The high R^2 value (0.9943) implied the existence of reasonable agreement between predicted and experimental values for explaining the 99.43% variation in particle size. The minimal difference between predicted R^2 (0.9735) and adjusted R^2 (0.9871) value suggested the adequacy of the selected model for the prediction of response. The value of adequate precision was found to be 41.308 (greater than 4 is desirable), suggesting an adequate signal to measure the signal independent of noise. Further, low value for coefficient of

variation (1.27 %) indicated high degree of precision and reliability of the model. Hence, this selected quadratic model can be used to navigate the design space [54, 179, 212].

Table 6.9 Statistical analysis results of lack of fit for particle size, EE and PDI of CS-SLNs

Source	Sum of Squares	df	Mean Square	F Value	p-value Prob > F	
Particle size						
Linear	6753.05	9	750.34	15.48	0.0090	-
2FI	5752.29	6	958.72	19.78	0.0061	-
Quadratic	53.53	3	17.84	0.37	0.7810	Suggested
Cubic	0.000	0	-	-	-	Aliased
Pure Error	193.87	4	48.47	-	-	-
Encapsulation efficiency						
Linear	226.28	9	25.14	38.56	0.0016	-
2FI	180.69	6	30.12	46.19	0.0012	-
Quadratic	7.86	3	2.62	4.02	0.1062	Suggested
Cubic	0.000	0	-	-	-	Aliased
Pure Error	2.61	4	0.65	-	-	-
PDI						
Linear	0.008478	9	0.00094	37.68	0.0016	-
2FI	0.006429	6	0.00010	42.86	0.0014	-
Quadratic	0.000433	3	0.00014	5.77	0.0617	Suggested
Cubic	0.000	0	-	-	-	Aliased
Pure Error	0.0001	4	0.00002	-	-	-

Statistical analysis revealed that concentration of lipid (X_1) affects positively, whereas concentration of surfactant (X_2) and organic phase/aqueous phase ratio (X_3) affect negatively on particle size. Also higher coefficient value (44.49) of concentration of

lipid (X_1) suggested that it had most significant effect on particle size followed by concentration of surfactant (X_2) and organic phase/aqueous phase ratio (X_3). While in case of the interactive effects between different independent variables, concentration of lipid and concentration of surfactant (X_1X_2) as well as concentration of lipid and organic phase/aqueous phase ratio (X_1X_3) had combined significant effect on particle size. It is visually discerned from 3D response surface plots and 2D contour plots as shown in Figure 6.4.

Concentration of lipid seems to be one of the most dominant parameters influencing the particle size of CS-SLNs owing to its direct effect on viscosity. Higher lipid concentration promotes the viscosity of organic phase, which reduces the stirring efficiency and thus poses resistance to emulsion droplet breakdown, resulting in larger particle. According to Stoke's low, the resultant density difference between aqueous and organic phase, at higher lipid concentration enhances the probability of particle contact by retarding the faster diffusion of organic solvent into external aqueous phase and subsequent coalescence [238, 239].

Alternatively, concentration of surfactant (X_2) holds inverse relationship with the particle size of CS-SLNs. The smaller-sized particles were formed with increased surfactant concentration might be the consequence of reduction of interfacial tension between organic and aqueous phase, which eventually formed smaller-sized droplets [240]. Higher surfactant concentration also imparts stabilization against aggregation by rapid covering on the surface of newly generated particles and thus protects from growing into bigger one [241]. Similarly, organic phase/aqueous phase ratio (X_3) negatively affects the particle size of CS-SLNs by diluting the lipid concentration at higher organic phase/aqueous phase ratio. Higher organic phase reduces the viscosity and thereby, effectively increases the shear stress to break down the emulsion

droplets. It also favors the faster diffusion of organic phase into aqueous phase and ultimately results in nucleation of smaller-sized emulsion droplets, and thus smaller sized particles [54, 214].

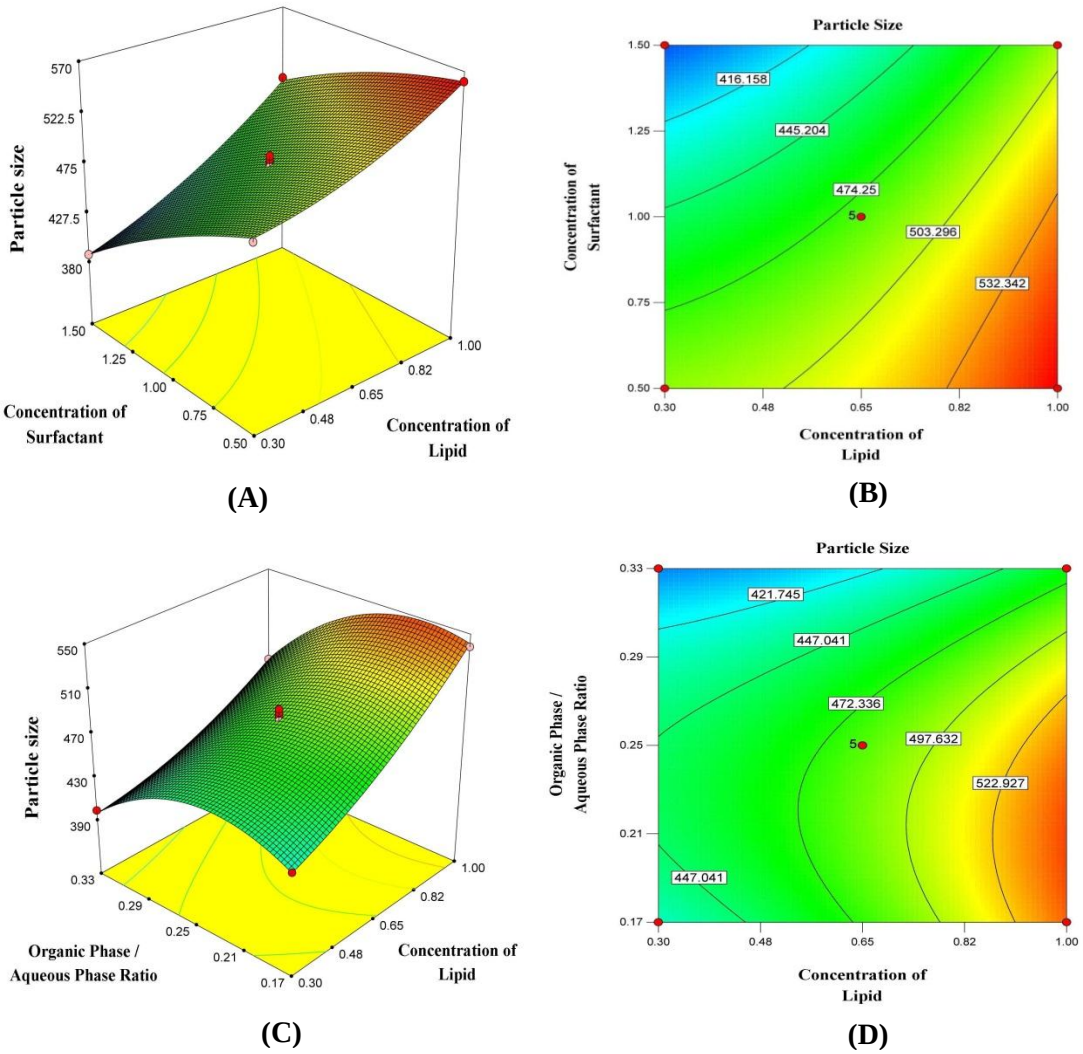

Figure 6.4 3D surface plots (A), (C) and 2D contour plots (B), (D) showing the effect of independent variables (concentration of lipid, concentration of surfactant and organic phase/aqueous phase ratio) on particle size of CS-SLNs

6.2.2.2.2 Influence of Independent variables on encapsulation efficiency

EE of CS-SLNs varies in the range of 12.5 $\pm$ 1.9 % to 35.2 $\pm$ 2.4 % for various factor's level combinations. The quadratic model was selected for the statistical analysis of influence of independent variables on EE of CS-PNs based on the lack of

fit test as shown in Table 6.9. The effect of the independent variables on EE (Y_2) can be explained by the following second-order quadratic equation (Eq (6.2)) in terms of coded variables.

$$Y_2 = 30.78 + 5.46X_1 - 5.53X_2 - 3.04X_3 + 3.38X_1X_2 - 2.69X_2^2 - 5.66X_3^2 \quad \text{Eq (6.2)}$$

Non-significant lack of fit value (p=0.1062; p>0.05) with F-value of 4.02 indicated that quadratic model is best fit to the independent variables for significantly describing the influence on the EE. Good correlation between experimental and predicted values was noticed as revealed by R^2 value of 0.9867. The minimal difference between predicted R^2 (0.8347) and adjusted R^2 (0.9695) value indicated the adequacy of the selected model for the prediction of response. The value of adequate precision was found to be 23.88 (greater than 4 is desirable), suggesting an adequate signal to measure the signal independent of noise. Further, low value for coefficient of variation (4.52 %) indicated high degree of precision and reliability of the model. Thus, the present quadratic model for EE can be used to navigate the design space [54, 179, 212].

Statistical analysis revealed that concentration of lipid (X_1) affects positively, whereas concentration of surfactant (X_2) and organic phase/aqueous phase ratio (X_3) affect negatively on EE of CS-SLNs. Also higher coefficient value (5.53) of concentration of surfactant (X_2) suggested that it had most significant effect on EE followed by concentration of lipid (X_1) and organic phase/aqueous phase ratio (X_3). While in case of the interaction effects between different independent variables, only concentration of lipid and concentration of surfactant (X_1X_2) had combined significant effect on EE. However, effect of independent variables on EE is lower than the effect on particle size. This is because of the lower coefficient value of the main effects and interaction

terms in the polynomial equation of EE compared with the polynomial equation of particle size [54, 179]. 3D response surface plots and 2D contour plots portraying the effect of independent variables on EE are shown in Figure 6.5.

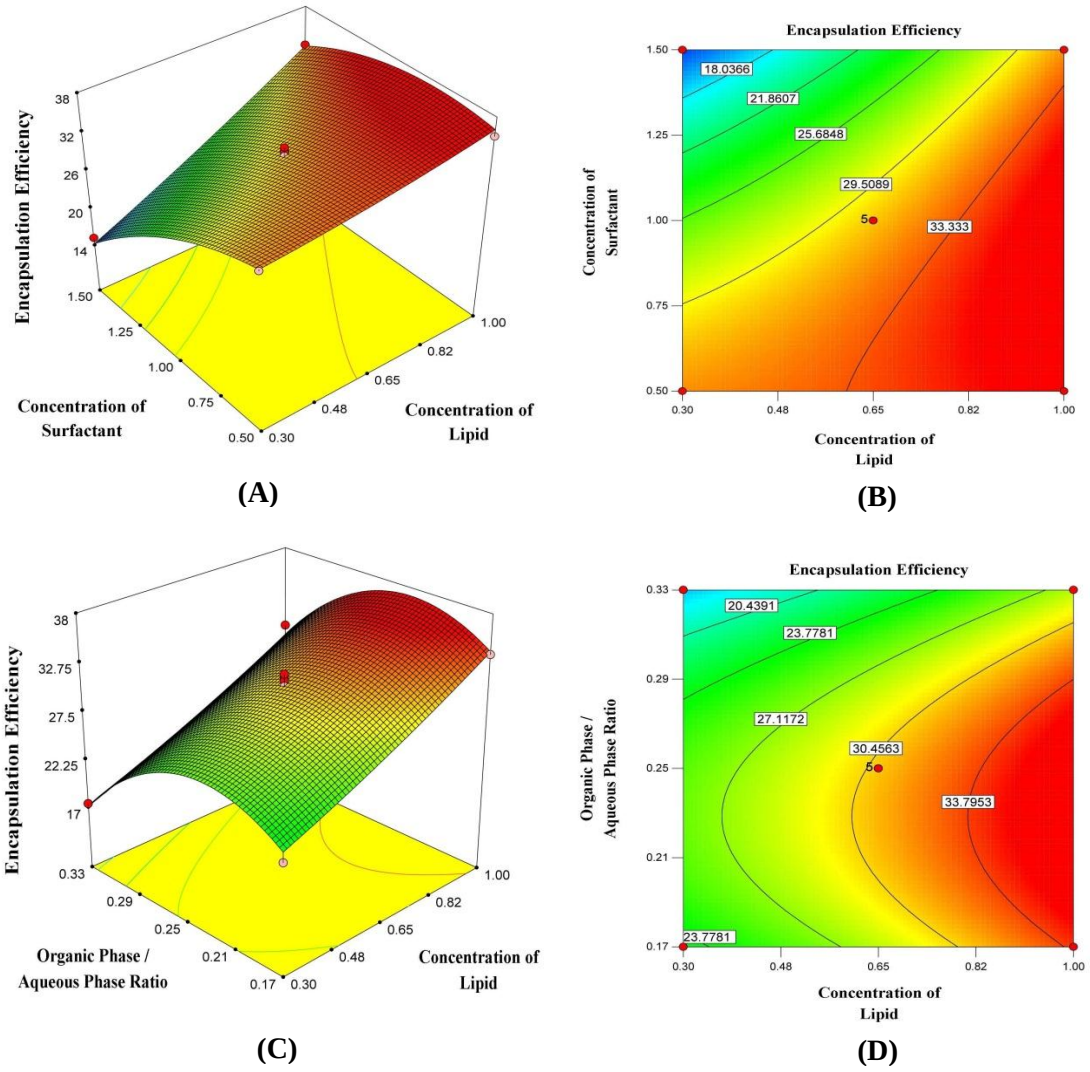

Figure 6.5 3D response surface plots (A), (C) and 2D contour plots (B), (D) showing the effect of independent variables (concentration of lipid, concentration of surfactant and organic phase/aqueous phase ratio) on encapsulation efficiency of CS-SLNs

The enhanced EE of CS-SLNs with a relative increase in the lipid concentration (X_1) was observed on account of more availability of lipid for encapsulating the CS. Increased lipid concentration also imparts viscous diffusional barrier at the interface

which restricts the outward movement of CS towards the external aqueous phase, leading to an increase in EE. Moreover, increased particle size at higher lipid concentration also favors high EE by increasing the diffusional path length [216, 242]. Conversely, the increase in surfactant concentration (X_2) resulted in the reduced EE of CS-SLNs. This could be explained by marked reduction in an interfacial tension, which ultimately increases CS partition into aqueous phase, contributing to substantial lowering of the EE [208, 217]. Likewise, significant reduction in EE noticed with raised organic phase/aqueous phase ratio (X_3) was ascribed to partition phenomenon, resulted from substantial lowering of viscosity, which would have hindered the drug retention inside the lipid matrix and have favored the drug partition in the external aqueous phase [54, 218].

6.2.2.2.3 Influence of independent variables on polydispersity index

The CS-SLNs exhibited relatively narrow particle size distribution in the range of 0.116 $\pm$ 0.042 to 0.386 $\pm$ 0.035 for selected level combination of different variables. Low PDI values nearer to 0 indicate the relative homogenous nature of the dispersion. The quadratic model was selected for the statistical analysis of influence of independent variables on PDI based on the lack of fit test as shown in Table 6.9. The second-order polynomial equation explaining the effect of the independent variables on PDI (Y_3) was obtained as follows in terms of coded variables (Eq (6.3)).

$$Y_3 = 0.24 + 0.062X_1 - 0.064X_2 - 0.046X_3 + 0.017X_1X_2 - 0.013X_1X_3 + 0.031X_1^2 - 0.022X_3^2 \quad \text{Eq (6.3)}$$

The F-value of 5.77 with the absence of lack of fit value (p=0.0617; p>0.05) for quadratic model proves the excellent adequacy for significantly describing the influence of independent variables on the PDI. The higher R^2 value of 0.9941

suggests that 99.41% of variation in PDI was best explained by the formulation variables. The minimal difference between predicted R^2 (0.9210) and adjusted R^2 (0.9864) value suggested the adequacy of the selected model for the prediction of response. The value of adequate precision was found to be 39.933 (greater than 4 is desirable), suggesting an adequate signal to measure the signal independent of noise. Further, low value for coefficient of variation (3.49 %) indicated high degree of precision and reliability of the model. Hence, the quadratic model can be considered for navigating the design space [54, 179, 212].

Statistical analysis revealed that concentration of lipid (X_1) affects positively, whereas concentration of surfactant (X_2) and organic phase/aqueous phase ratio (X_3) affect negatively on PDI of CS-SLNs. Also higher coefficient value (0.064) of concentration of surfactant (X_2) suggested that it had most significant effect on PDI of CS-SLNs followed by concentration of lipid (X_1) and organic phase/aqueous phase ratio (X_3). While in case of the interactive effects between different independent variables, concentration of lipid and concentration of surfactant (X_1X_2) as well as concentration of lipid and organic phase/aqueous phase ratio (X_1X_3) had combined significant effect on EE. However, effect of independent variables on PDI is lowest than the effect on particle size and EE. This is because of the lower coefficient value of the main effects and interaction terms in the polynomial equation of PDI compared with the polynomial equation of particle size and EE [54, 179]. 3D response surface plots and 2D contour plots portraying the effect of independent variables on PDI of CS-SLNs are shown in Figure 6.6.

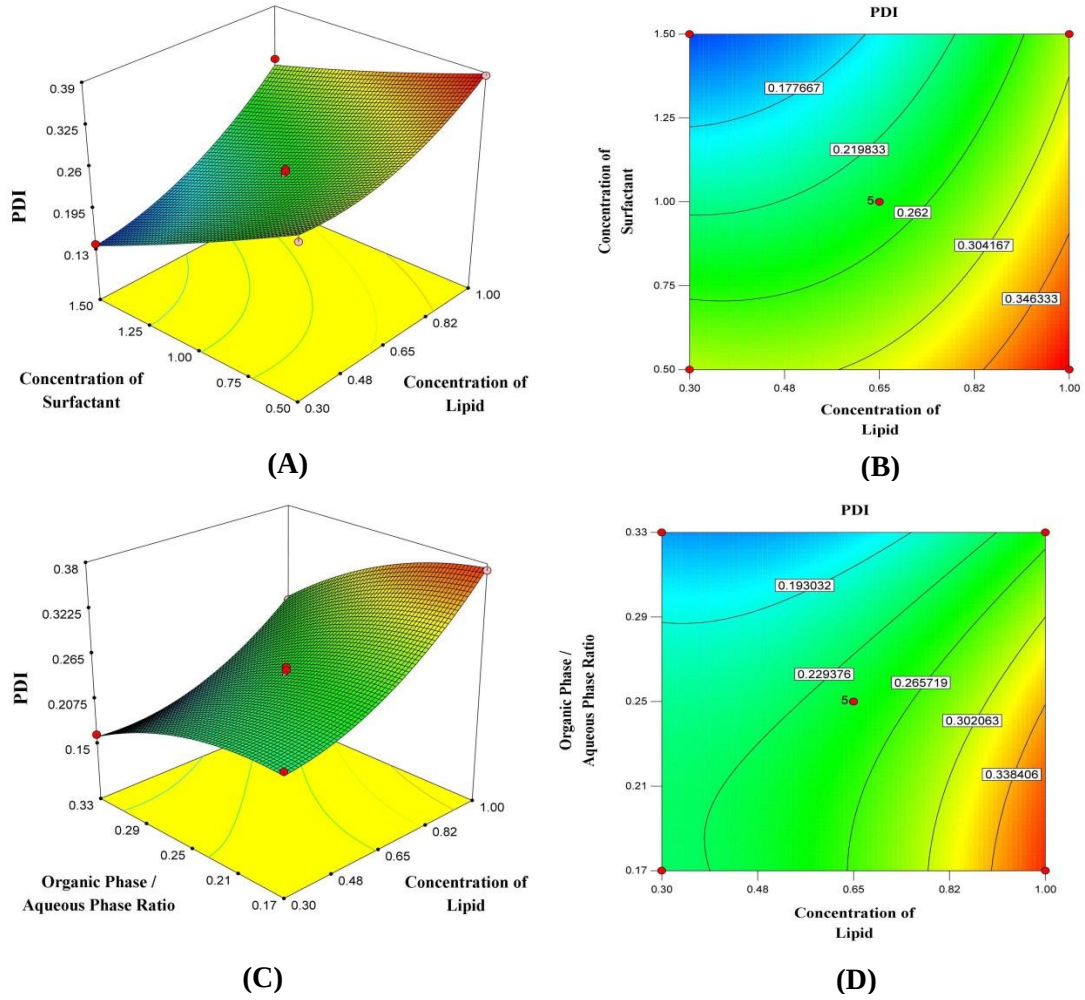

Figure 6.6 3D response surface plots (A), (C) and 2D contour plots (B), (D) showing the effect of independent variables (concentration of lipid, concentration of surfactant and organic phase/aqueous phase ratio) on PDI of CS-SLNs

While evaluating PDI as response, significant increment was observed as a consequence of increase in lipid concentration (X_1) might be due to the shortening of time required for the nucleation of the lipid particles compared to time required for covering the surface of lipid particles by surfactant and thus, results in lack of complete surface covering. This ultimately enforces the formation of different-sized aggregates and thereby, potentiates polydispersity [214]. Oppositely, the reduction in polydispersity was noticed with an increase in both, concentration of surfactant (X_2) and organic phase/aqueous phase ratio (X_3) might be attributed to the reduction of

interfacial tension, which ensures a good emulsification process as well as dilution of lipid concentration as explained earlier, which in turn would have enforced the monodispersity [49, 54].

6.2.2.2.4 Optimization of CS-SLNs using desirability function

Optimization of formulation by considering all the objectives at a time is difficult owing to opposite effect of various independent variables. The optimum level of one independent variable might result in an inverse effect for other independent variable. Hence, desirability approach was probed for numerical optimization of all the three dependent variables simultaneously, by applying constraints to acquire optimized CS-SLNs.The levels of different independent variable which would yield maximum EE with minimum particle size and PDI were determined using Design-Expert® software. In order to optimize and evaluate the predictive power of experimental design and to confirm the validity of the optimization process, the new batch of CS-SLNs was prepared under the optimal conditions by considering the predicted levels of respective independent variables. Table 6.10 shows the predicted values of dependent variables and levels of independent variables along with the experimental results. The desirability of the optimized CS-SLNs was 0.636. The close proximity with low percentage of bias between predicted results and experimental results reaffirmed the reliability of prediction potential of QbD approach, using Box-Behnken experimental design for statistical optimization of desirable CS-SLNs [49, 179, 182, 183]. Optimized CS-SLNs were further selected for various *in-vitro* and *in-vivo* characterizations.

Table 6.10 Comparison of experimental and predicted values of optimized CS-SLNs with its desirability generated by Design expert®

Independent variables	Optimized levels		
Concentration of lipid (X_1)	0.61 % w/v		
Concentration of surfactant (X_2)	1.14 % w/v		
Organic phase/Aqueous phase ratio (X_3)	0.30		
Results			
	Experimental values	**Predicted values**	**% Bias***
Particle size (nm)	428 ± 4.6	432.90	1.13
Encapsulation efficiency (%)	24.84 ± 0.56	24.06	-3.24
Polydispersity index (PDI)	0.175 ± 0.048	0.182	3.84
Overall Desirability	0.636		
Drug loading (%)	3.2 ± 0.41		
Zeta potential (mV)	(-) 24.4 ± 2.6		

**Bias was calculated as [(predicted value-experimental value)/predicted value] X 100;*
All results are shown as mean ±S.D; n=3.

6.2.3 Characterizations of CS-SLNs

6.2.3.1 Solid state characterizations

6.2.3.1.1 Fourier transform infrared spectroscopy (FTIR) study

FTIR study was performed in order to evaluate chemical stability and to identify the significant change, if occurs during the encapsulation of CS inside the SLNs. The FTIR spectra for pure CS, GMS, PVA and optimized CS-SLNs are shown in Figure 6.7. As depicted in Figure 6.7 (a), FTIR spectra of CS exhibited the characteristic basic peaks corresponding to C=O (1639.54 cm^{-1}), asymmetric COO^- (1573 cm^{-1}),

symmetric COO^- (1410 cm^{-1}), O-H (3416 cm^{-1}), C-H alkane (2880 cm^{-1}) and aromatic C-H (1477 cm^{-1}). Moreover, the vibrations within a molecule were noticed through the large number of characteristic bands in fingerprint region (1400–600 cm^{-1}) [43, 45, 49]. The characteristic bands of GMS were attributed to C-H stretching (2840-2960 cm^{-1}), C-H bending (850-700 cm^{-1}) and C=O stretching (1730 cm^{-1}) as depicted in Figure 6.7 (b) [237]. FTIR spectra of PVA (Figure 6.7 (c)) depicted all the major peaks, including C-H stretching (2840-3000 cm^{-1}) from alkyl group and O-H stretching from the hydrogen bonds (intermolecular and intramolecular) (3200-3550 cm^{-1}). It also showed the peaks related to C=O stretching together with C-O stretching from the acetate group (1750-1735 cm^{-1}) [206].

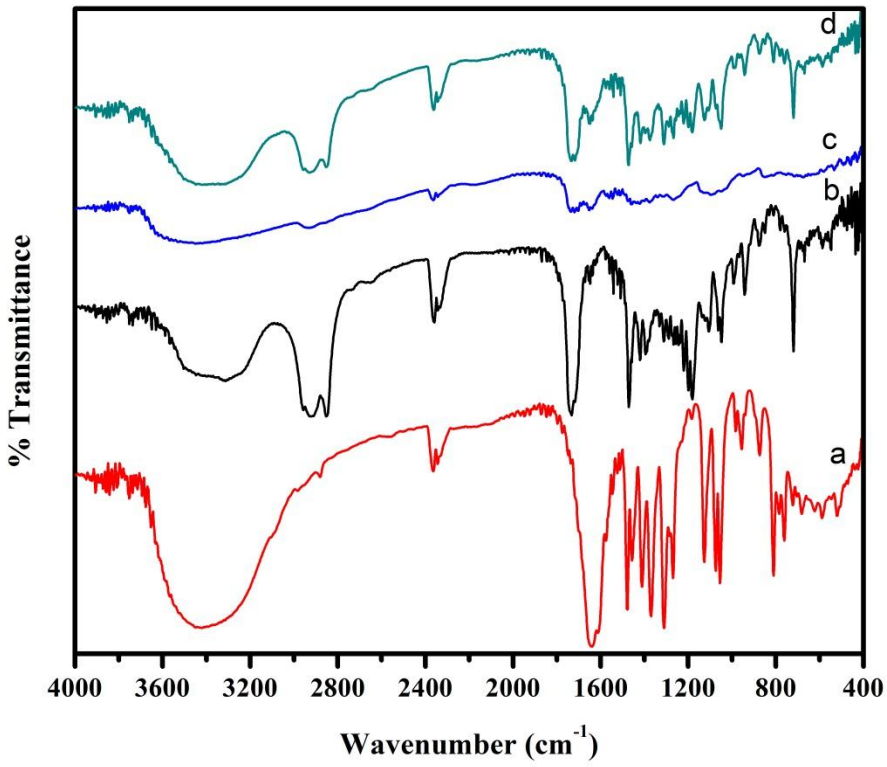

Figure 6.7 FTIR spectra of (a) CS, (b) GMS, (c) PVA and (d) optimized CS-SLNs

In FTIR spectra of optimized CS-SLNs (Figure 6.7 (d)), the appearance of all characteristic peaks of CS at nearly same wavenumber in optimized CS-SLNs as appeared in pure CS without changing their positions, confirmed the successful encapsulation of CS inside the matrix of the SLNs without any kind of modification during the encapsulation process [49, 221].

6.2.3.1.2 Differential scanning calorimetry (DSC) study

DSC thermogram of pure CS, GMS, PVA and optimized CS-SLNs are depicted in Figure 6.8.

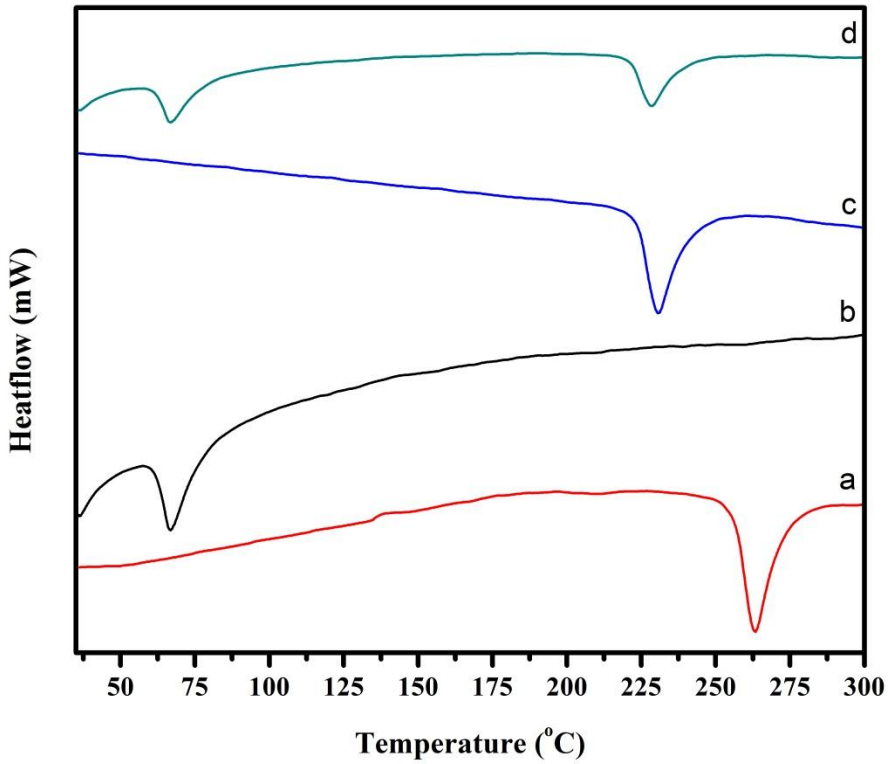

Figure 6.8 DSC thermograms of (a) CS, (b) GMS, (c) PVA and (d) optimized CS-SLNs

The pure CS displayed sharp endothermic peak at 264 ^{o}C corresponding to its melting point, which indicates about its crystalline nature. Further, any peaks due to release of

absorbed moisture or nonstructural water as well as solid state transitions were not identified [49, 149, 210]. GMS and PVA showed sharp endotherm at 62 ^{o}C and 226 ^{o}C corresponding to their respective melting points. However, the endothermic peak of CS was completely disappeared in the thermogram of optimized CS-SLNs (Figure 6.8 (d)), which indicates the physical state transformation and molecular inclusion of CS inside the matrix of SLNs in an amorphous or disordered-crystalline drug phase. Hence, it seemed that lipid matrix has entirely covered the CS in an amorphous form during the encapsulation process [207, 210, 224].

6.2.3.1.3 Powder X-ray diffractometry (PXRD) study

Powder X-ray diffractogarms of pure CS, GMS, PVA, their physical mixture and optimized CS-SLNs are depicted in Figure 6.9. The powder X-ray diffraction pattern of pure CS exhibited its traits of highly crystalline nature by numerous, distinctive sharp diffraction peaks, observed at a 2θ value of 8^{o}, 9.83^{o}, 11.5^{o}, 14^{o}, 16.9^{o}, 19.7^{o}, 24.3^{o}, 26.6^{o} and various minor peaks up to 35^{o} as illustrated in Figure 6.9 (a) [45, 49, 149]. Two prominent crystalline peaks at a 2θ value of 19^{o} and 24^{o} with high intensity was observed for GMS due to scattering from the crystalline region. The PXRD pattern of PVA showed small diffuse peaks with broad halo. The crystallinity of the CS was also retained in the physical mixture of CS along with GMS and PVA as observed by its sharp peaks in diffractogram of the physical mixture. Since GMS and PVA exhibited no any characteristic diffraction peaks, the crystalline peaks must be originated from the crystalline region of CS, which indicates the retention of CS crystallinity in physical mixture, without any interactions (Figure 6.9 (d)). Whereas, marked difference was observed in the PXRD pattern of optimized CS-SLNs (Figure 6.9 (e)), which showed absence of crystalline peaks of CS along with broad and diffused peaks. The results clearly confirmed the encapsulation of CS in an

amorphous molecular dispersion form within the lipid matrix [207, 210, 226]. PXRD results are in good agreement with the results demonstrated by DSC, confirming the homogeneous and complete encapsulation of CS inside the lipidic matrix of the nanoparticles [39, 45, 224].

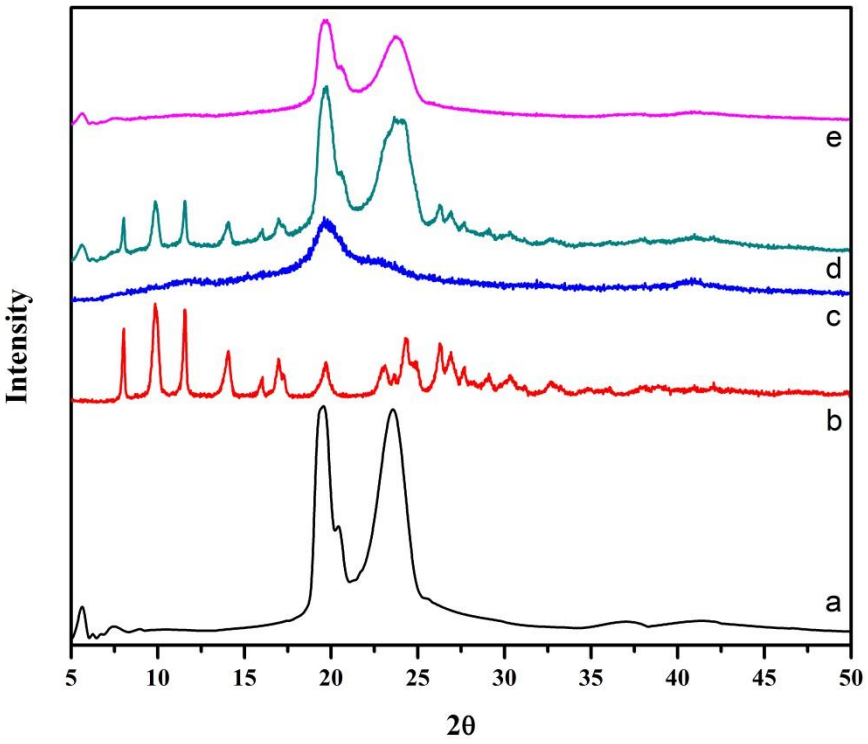

Figure 6.9 PXRD patterns of (a) GMS, (b) CS, (c) PVA, (d) physical mixture and (e) optimized CS-SLNs

6.2.3.2 Shape and surface morphology

6.2.3.2.1 High resolution transmission electron microscopy (HR-TEM)

The shape and surface morphology of the optimized CS-SLNs was determined by employing HR-TEM. The HR-TEM micrograph of CS-SLNs (Figure 6.10 (A)) showed discrete, spherical shaped particles having uniform size distribution with low polydispersity. The surface morphology of CS-SLNs exhibited smooth surface

without any rough pores. The particle size obtained by HR-TEM was well correlated with the particle size measured by dynamic light scattering technique, in which most of them are smaller than 500 nm.

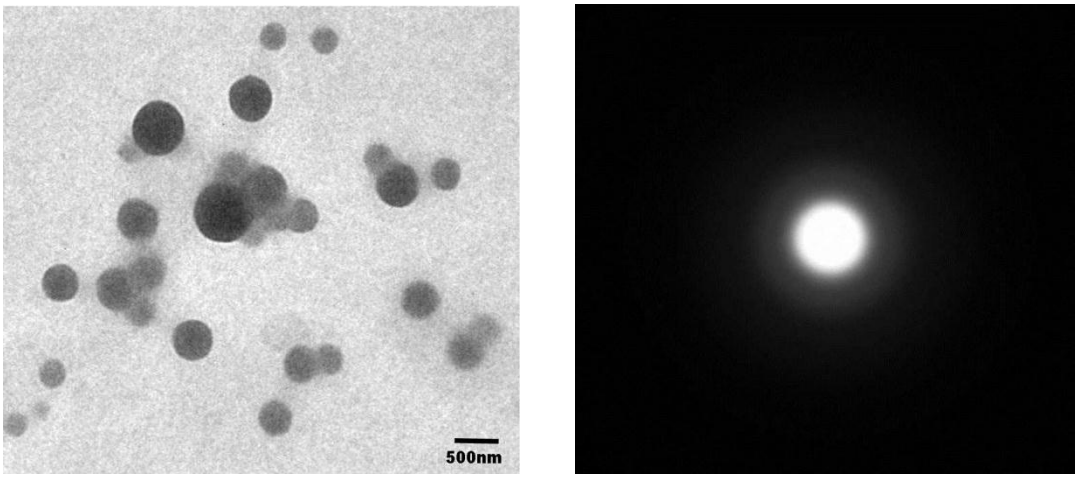

(A) **(B)**

Figure 6.10 (A) HR-TEM image of optimized CS-SLNs; (B) Electron diffraction pattern of optimized CS-SLNs

Further, the physical state of CS inside the lipidic matrix was studied by electron diffraction (ED) pattern. The ED pattern (Figure 6.10 (B)) obtained by visualizing CS-SLNs revealed the existence of smooth diffraction halo without any bright spots in the circular ring pattern, indicating that CS was encapsulated homogeneously as an amorphous form inside the SLNs [49, 198, 226], which further substantiates the inference deduced from DSC and PXRD results.

6.2.3.2.2 Atomic force microscopy (AFM)

The surface morphology of optimized CS-SLNs was further confirmed by AFM study. The topographic and 3D AFM micrographs of CS-SLNs, generated by the atomic level interaction between a sharp probing tip and the surface of CS-SLNs with a spatial resolution up to 0.01 nm, are depicted in Figure 6.11 (A) & (B).

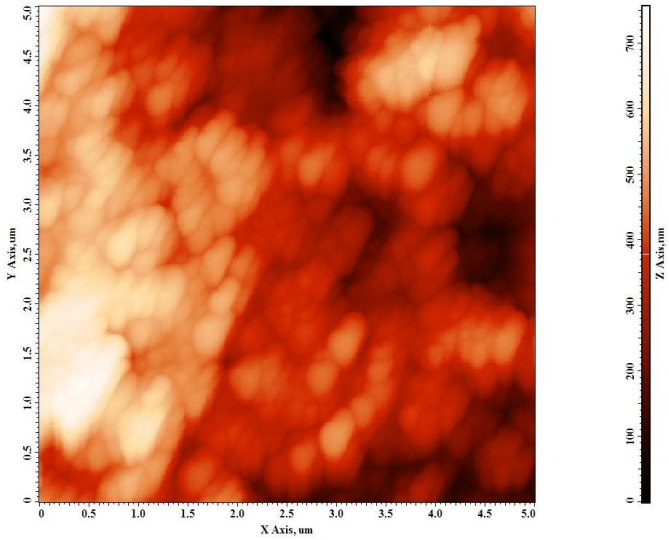

(A)

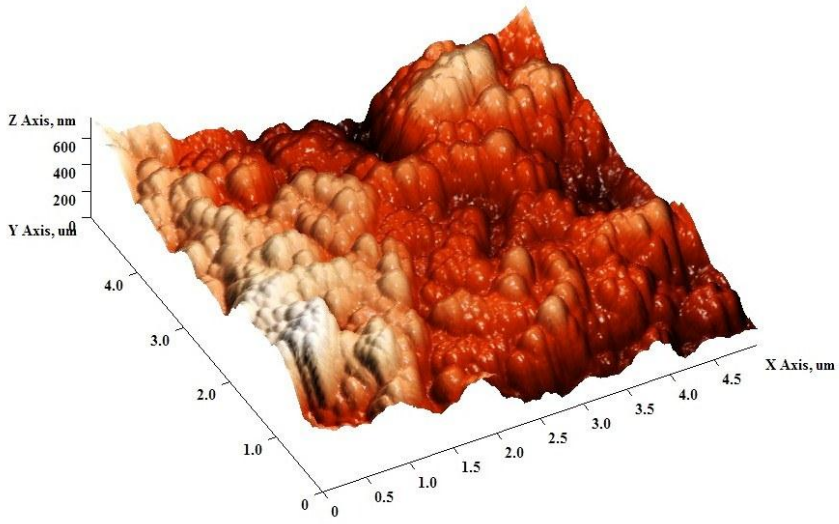

(B)

Figure 6.11 AFM images of optimized CS-SLNs (A) 2D micrograph and (B) corresponding 3D micrographs.

The particle size and surface morphology of CS-SLNs revealed by AFM was in accordance with the results of HR-TEM study. AFM images generated by direct analysis of originally hydrated CS-SLNs sample, demonstrated uniform spherical shaped CS-SLNs having smooth surface without any rough crevices or pores.

AFM micrographs displayed the well separated and distinct CS-SLNs in the nanometric size range with low polydispersity. The probable reason for smooth surface could be the covering of surfactant molecules over the outer surface of SLNs, which has resealed the pores or crevices generated by the diffusion of organic solvent during the preparation [23, 188].

6.2.3.3 *In-vitro* drug release study

In-vitro drug release profile of CS from CS-SLNs showed the biphasic release pattern in phosphate buffer pH 7.4 as illustrated in Figure 6.12. The optimized CS-SLNs exhibited around 95% drug release at the end of 24 hr. The surface adsorbed CS showed an initial burst release (nearly 20% drug release) within 1 hr due to faster diffusion followed by extended release over 24 hr due to hydration and swelling of CS-SLNs (Table 6.11). Hydration causes substantial increment in the diffusional path length, which eventually slowdowns the diffusion of drug molecules form the nanoparticles [227]. Additionally, the extended release behaviour of CS was also correlated to the homogeneous encapsulation within the SLNs, which decelerates the faster immobilization from lipidic matrix and controls the release. These results indicated that the release of CS from CS-SLNs was mainly governed by a combination of process, i.e., drug diffusion rate from the hydrophobic long carbon chain of lipid and fluidization as well as integrity of carrier lipidic matrices [49, 111, 198].

Table 6.11 *In-vitro* drug release data of the optimized CS-SLNs in phosphate buffer pH 7.4

Time (hr)	Cumulative % drug release
0	0
1	24.13 ± 2.53
2	27.76 ± 0.87
3	30.87 ± 0.84
4	36.89 ± 1.39
5	41.80 ± 0.55
6	47.26 ± 1.12
7	51.06 ± 0.84
8	58.84 ± 0.89
10	66.15 ± 1.57
12	73.10 ± 1.15
18	88.75 ± 2.37
24	95.97 ± 1.38

All values reported are mean ± SD, (n=3)

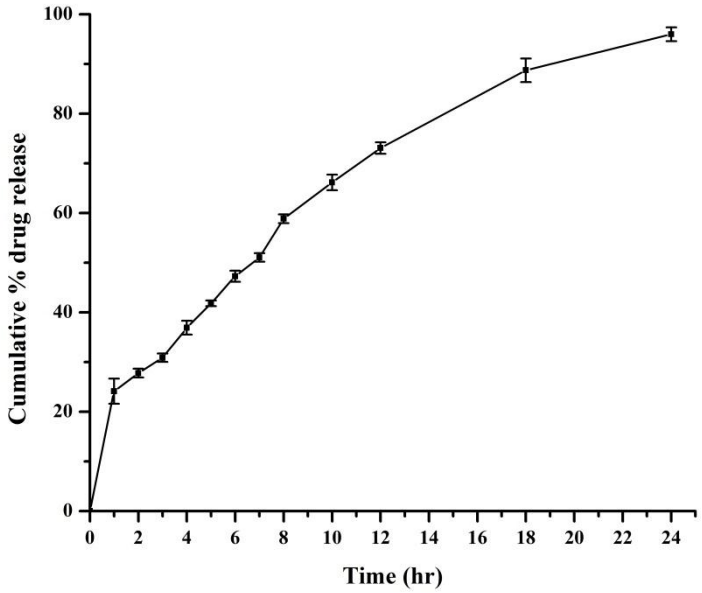

Figure 6.12 *In-vitro* drug release profile of optimized CS-SLNs in phosphate buffer pH 7.4 (vertical bar represents ± S.D; n=3)

The rate and extent of drug release can be easily correlated to the partition coefficient of the drug. Furthermore, the release kinetics and mechanism was determined by fitting different release kinetic models (i.e., zero order, first order, Higuchi model and Korsmeyer-Peppas model) to the *in-vitro* drug release profile of CS-SLNs. Results of *in-vitro* release kinetic analysis suggested that the release of CS from CS-SLNs was best explained by Higuchi model showing diffusion, based release process (highest R^2 value compared to other kinetic models as shown in Table 6.12). Further, the release exponent (n) value obtained by fitting Korsmeyer-Peppas model was found to be 0.488, which is suggestive that the drug release occurred through diffusion controlled release process from the lipid matrix based on Fick's law ($n<0.5$ for fickian diffusion) [191, 192]. As CS is the hydrophilic drug molecule, its release follows higuchi model, which is likely complies with the previously reported scientific literature for the hydrophilic drug release from different carriers [243]. Hence, it is possible to provide loading dose due to initial burst release followed by maintenance dose due to sustained release by administering CS-SLNs, in order to achieve fluctuation free steady state CS plasma level [49].

Table 6.12. Release kinetic models for simulation of release behaviour of CS from optimized CS-SLNs in phosphate buffer pH 7.4

Batch	Zero Order	First Order	Higuchi Model	Korsemeyer-Peppas model
Optimized CS-SLNs	$R^2 = 0.9458$ $K_z = 3.351$	$R^2 = 0.8476$ $K_F = 0.0605$	$R^2 = 0.9837$ $K_H = 20.527$	$R^2 = 0.9686$ $K_P = 20.413$ $n = 0.4884$

6.2.3.4 Accelerated and real time storage stability study

The ability of any colloidal system to remain stable against environmental changes is of prime requirement to ensure its final performance in terms of its *in-vivo* fate. Nanoparticles have very high tendency to agglomerate owing to their large surface-area-to-volume ratio, which results in the increase in particle size after longer periods of storage. Changes in the physical appearance, color, odor, taste, or texture of the formulation indicate the instability. The stability and intactness of CS-SLNs was assessed over a period of 6 month at room temperature (25 $\pm$ 2 ^{o}C), refrigerated condition (4 $\pm$ 1 ^{o}C), and accelerated condition (40 $\pm$ 2 ^{o}C/75 $\pm$ 5 % RH). The physical appearance and physicochemical attributes (i.e., particle size, EE and PDI) were chosen as stability indicating parameters. The changes in the physicochemical properties of the CS-SLNs during the stability study over the period of 6 months are depicted in Figure 6.13. There was no any significant noticeable change in the physical appearance (i.e., lump formation and discoloration) observed at different environmental condition during the study. Depositions formed on the base of container during storage were easily redispersible on mere shaking.

CS-SLNs stored at refrigerated condition (4 $\pm$ 1 ^{o}C), showed insignificant change (p>0.05) in their particle size, PDI and EE. However, significant (p<0.05) increase in particle size was observed for CS-SLNs, stored at room temperature (25 $\pm$ 2 ^{o}C). Interestingly, EE and PDI were remained unaffected and preserved their intactness in the formulation.

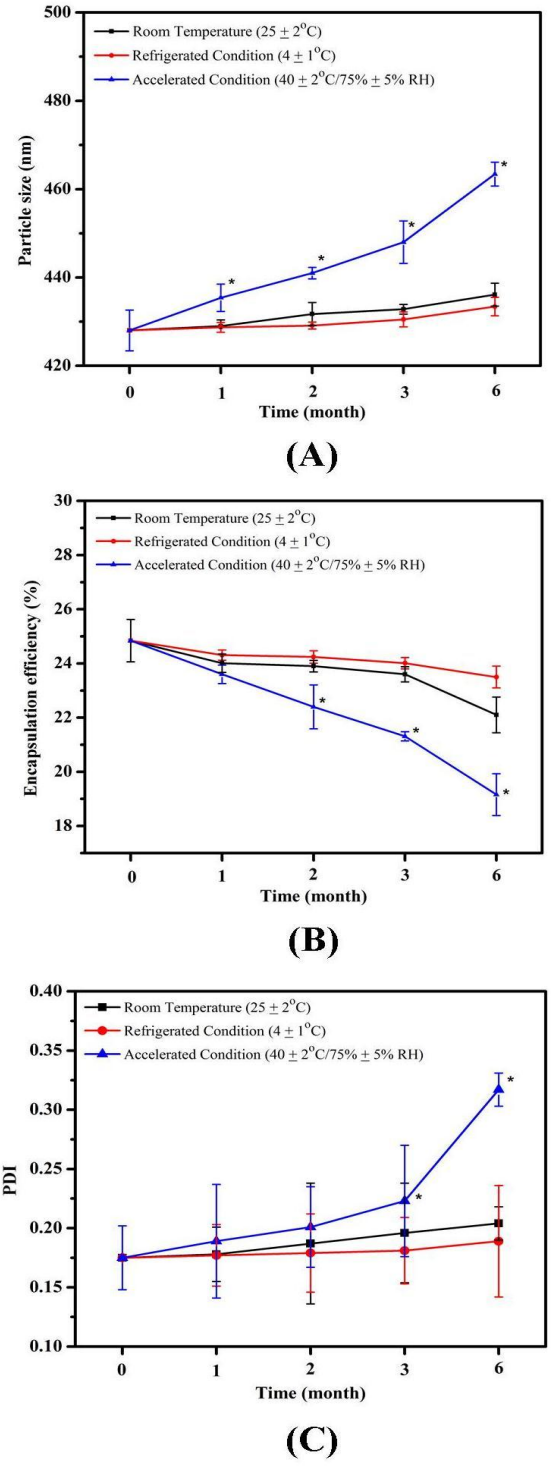

Figure 6.13 Effect on (A) particle size, (B) encapsulation efficiency and (c) PDI of optimized CS-SLNs stored at different environmental conditions over different time interval (vertical bars represent ± SD; n=3); *significant at $p<0.05$ compared with 0 time

In case of CS-SLNs stored at accelerated condition (40 ± 2 °C/75 ± 5 % RH), the significant change (p<0.05) was noticed for particle size, PDI and EE, suggesting instability due to aggregation of the CS-SLNs. The substantial aggregation of CS-SLNs might be as a result of degradation and partial melting of the lipidic material, which would have expelled the drug molecule from lipidic nanostructures [23]. Therefore, it is strongly recommended that the designed CS-SLNs should be stored at refrigerated condition (4 ± 1 °C), to hold the pharmaceutical properties as well as hydrophilic drug inside nanostructures for safe and effective long-term use [49, 193, 228, 229].

6.2.3.5 *Ex-vivo* intestinal permeation study

Non-everted intestinal sac method was employed for assessing the permeation potential of CS and CS-SLNs across the rat intestine. The *ex-vivo* intestinal permeation of CS-SLNs and CS solution along with their apparent permeability coefficient (Papp) at pH 7.4 is depicted in Figure 6.14. The CS-SLNs exhibited significant improvement (p<0.05) in CS permeation across excised rat intestinal membrane at each time point compared to pure CS solution (Table 6.13). The apparent permeability coefficient for CS was found to be 0.909 (± 0.049) × 10^{-5} cm/s, due to poor permeation across rat intestine as a result of high hydrophilicity [43, 45], whereas apparent permeability coefficient for CS-SLNs was found to be 2.696 (± 0.315) × 10^{-5} cm/s (Figure 6.15).

Table 6.13 *Ex-vivo* permeation data of the CS solution and optimized CS-SLNs across rat intestinal membrane

Time (min)	Cumulative % drug permeated	
	CS solution	CS-SLNs
0	0	0
15	1.21 ± 0.039	2.17 ± 0.72
30	2.40 ± 0.021	3.10 ± 0.75
45	3.33 ± 0.053	5.25 ± 0.58
60	4.39 ± 0.052	7.80 ± 1.62
90	4.98 ± 0.083	12.28 ± 2.33
120	5.71 ± 0.539	18.63 ± 1.91
180	6.78 ± 0.504	24.86 ± 2.00
240	7.71 ± 0.588	31.58 ± 2.53

All values reported are mean ± SD, (n=3).

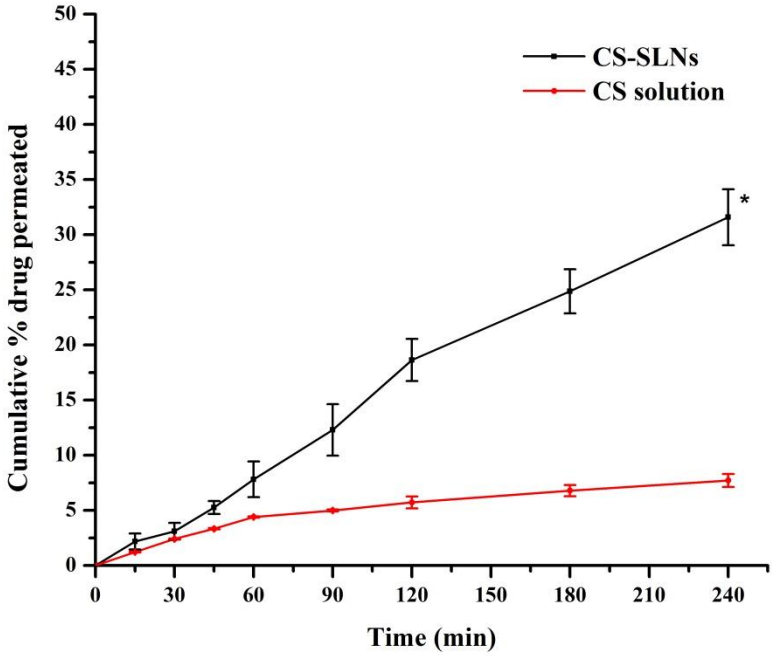

Figure 6.14 *Ex-vivo* permeation study of CS-SLNs and CS solution across rat intestinal membrane. Vertical bars represent ± SD; n=3, *significant at $p<0.05$ compared with CS solution (Unpaired student t-test)

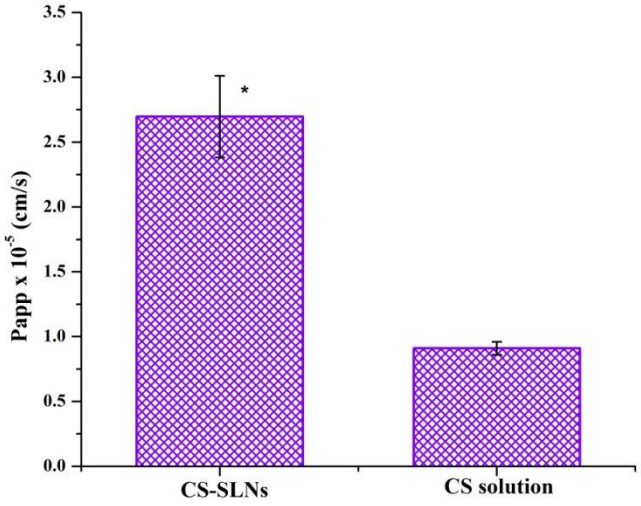

Figure 6.15 Apparent permeability coefficients (Papp) for CS from CS-SLNs and CS solution. Vertical bars represent ± SD; n=3, *significant at $p<0.05$ compared with CS solution (Unpaired student t-test)

The significant higher ($p<0.05$) permeability for the CS-SLNs is likely owing to its nanosize structure, which would have imparted larger specific surface area and their specific absorption mechanisms across the GIT. As CS was encapsulated within SLNs, the transport of CS-SLNs through trancellular pathway via enterocytes and selective uptake by M cells of PP in lymphoid tissues across the GIT, resulted in about ~2.96 fold enhanced permeation contrast to CS solution [106, 107]. Moreover, the lipidic nature of the CS-SLNs also might be responsible for better CS permeation which in turn eventually reflected by the greater CS concentration in receptor compartment. Thus, the enhancement in GIT permeation confirmed the role of enterocytes and M cells of PP in the intestinal permeation enhancement [24, 49, 232].

6.2.3.6 *In-vivo* intestinal uptake study

In-vivo intestinal uptake study was performed in rats to visualize the permeation potential of CS-SLNs across the GIT. The confocal microscopic images of cross-

sections of isolated rat intestinal mucosal tissue, after oral administration of coumarin-6 loaded CS-SLNs to the overnight fasted rats are shown in Figure 6.16. The visualization exhibited the various stages of internalization and distribution of coumarin-6 loaded CS-SLNs inside the villi as well as PP of the follicle-associated epithelium via strong green colored fluorescence, which confirmed that effective endocytosis took place inside the enterocytes.

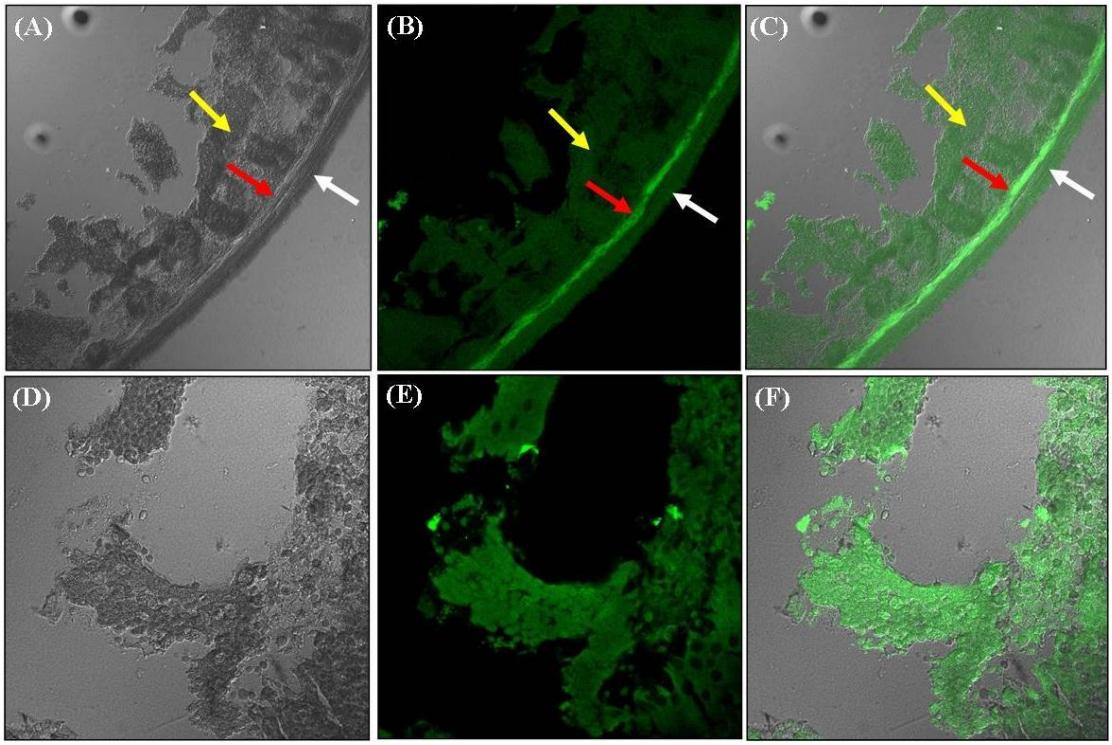

Figure 6.16 Confocal laser scanning micrographs of rat intestine, showing uptake and transport of coumarin-6 labelled CS-SLNs into the tissues, underlying the absorptive cells, after 2 hr of oral administration. (A) DIC image; (B) Fluorescent image; and (C) Merge of fluorescent and DIC image scanned at 10× plain. (D) DIC image; (E) Fluorescent image; and (F) Merge of fluorescent and DIC image scanned at 40× plain using emersion oil objective. Yellow, red and white arrows indicate the mucosal, submucosal, and muscular regions of rat intestine, respectively

The absorption of CS-SLNs occurs in rat follicular mucosa (PP) as well as non-follicular mucosa (normal enterocytes) as visualized in CLSM images. No fluorescence was observed in the lumen or mucus layer. The intriguing results demonstrated the lymphatic transport of CS-SLNs via transcellular pathway through enterocytes and endocytosis by M cells of PP [39, 45, 106, 196]. Additionally, the surfactant used in formulation of CS-SLNs (i.e., PVA) also caters mucoadhesivity to CS-SLNs which might have helped in improving the residence time of CS-SLNs with intestine and resulted in the improved intestinal permeation by facilitating particulate interaction [24]. As CS was encapsulated within CS-SLNs while permeating across GIT, it would have resulted in enhancement of absorption of CS and further, strengthens the finding of *ex-vivo* studies. Hence, it can be concluded that SLNs play an important role in the facilitating the CS absorption to systemic circulation through the intestinal membrane [49, 233, 234].

6.2.3.7 *In-vivo* pharmacokinetic study

The plasma drug concentration-time profiles obtained after the single dose oral administration of the CS solution and CS-SLNs in rats (20 mg/kg) are depicted in Table 6.14 and Figure 6.17. Various pharmacokinetic parameters of pure CS solution and CS-SLNs obtained by non-compartmental analysis are summarized in Table 6.15. As can be seen from the mean plasma drug concentration–time curve, oral administration of CS solution resulted into faster appearance of CS in blood. CS-SLNs, on the other hand, displayed entirely different pharmacokinetics.

Table 6.14 Plasma drug concentration time profile data of CS solution and CS-SLNs following single dose oral administration in rats

Time (hr)	Plasma concentration of CS (ng/ml)	
	CS solution	CS-SLNs
0	0	0
0.25	11.42 ± 1.36	6.92 ± 0.54
0.5	50.59 ± 4.30	37.26 ± 3.97
1	112.23 ± 5.90	69.66 ± 5.84
2	70.08 ± 2.86	146.84 ± 4.24
4	28.75 ± 2.10	83.55 ± 3.72
8	ND	35.46 ± 4.20
12	ND	7.84 ± 1.20
24	ND	ND

All values reported are mean ± SEM, (n=6); ND: Not detected

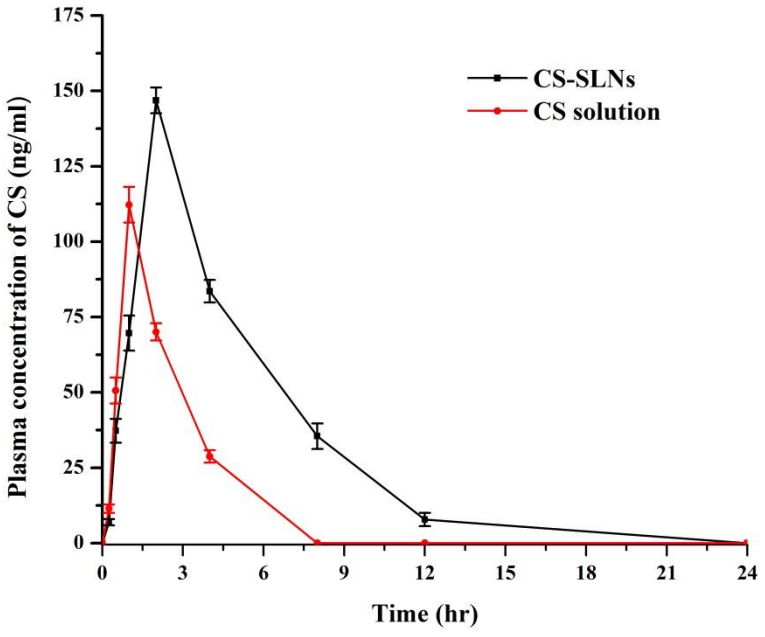

Figure 6.17 Plasma drug concentration time profile of CS-SLNs and CS solution following single dose oral administration in rats; Dose: 20 mg/kg (vertical bars represent ± SEM; n=6)

Non-compartmental analysis of CS plasma concentrations exhibited ~1.3 fold increments in C_{max} for CS-SLNs with respect to pure CS solution. The higher C_{max} for CS-SLNs can be due to enhanced permeation thereby, absorption across GIT by virtue of their smaller size and hydrophobic surfaces [27, 226]. The T_{max}, $T_{1/2}$ and MRT obtained with CS-SLNs were significantly higher than those obtained with pure CS solution. The MRT of CS-SLNs is about ~1.70 times greater that with CS solution, indicating prolonged stay of CS in body by incorporating into SLNs [106, 107]. The $T_{1/2}$ of CS is also increased from ~1.52 hr (CS-solution) to ~2.41 hr (CS-SLNs) following oral administration.

Table 6.15 Pharmacokinetic parameters of CS and CS-SLNs following single dose oral administration in rats (Dose: 20 mg/kg)

Parameters	CS solution	CS-SLNs
C_{max} (ng.ml^{-1})	112.23 ± 5.90	146.84 ± 4.24*
T_{max} (hr)	1 (± 0)	2 (± 0)
AUC_{0-24h} (ng.hr.ml^{-1})	232.16 ± 12.31	662.36 ± 19.97*
$AUC_{0-\infty}$ (ng.hr.ml^{-1})	295.53 ± 17.79	694.73 ± 29.38*
$T_{1/2}$ (hr)	1.52 ± 0.02	2.41 ± 0.23*
MRT (hr)	2.79 ± 0.03	4.77 ± 0.31*
Fr	1	2.86 ± 0.08*

**significant values at $p<0.05$ compared with CS solution (Unpaired student t-test); All values reported are mean ± SEM, (n=6).*

The values of AUC_{0-24hr} and $AUC_{0-\infty}$ for CS-SLNs were significantly higher ($p<0.05$) compared to pure CS solution, indicating the significant increase in the bioavailability of CS. The relative bioavailability of CS-SLNs was found to be ~2.86 fold higher with respect to CS solution upon single dose oral administration. Enhancement of oral

bioavailability might be attributed to the nano-sized structure and increased surface area, which would have enhanced systemic absorption of CS-SLNs through selective lymphatic uptake by M cells of PP and trancellular transport through enterocytes [49, 198, 235, 236]. Results coupled with confocal microscopic study corroborate well with the findings of *ex-vivo* studies and further confirms the hypothesis.

6.2.3.8 *In-vivo* mast cell stabilizing activity

The results of mast cell stabilizing activity in the rats are summarized in the Table 6.16. The degradation of the isolated peritoneal mast cells in different groups, after incubation with the compound 48/80 is depicted in Figure 6.18.

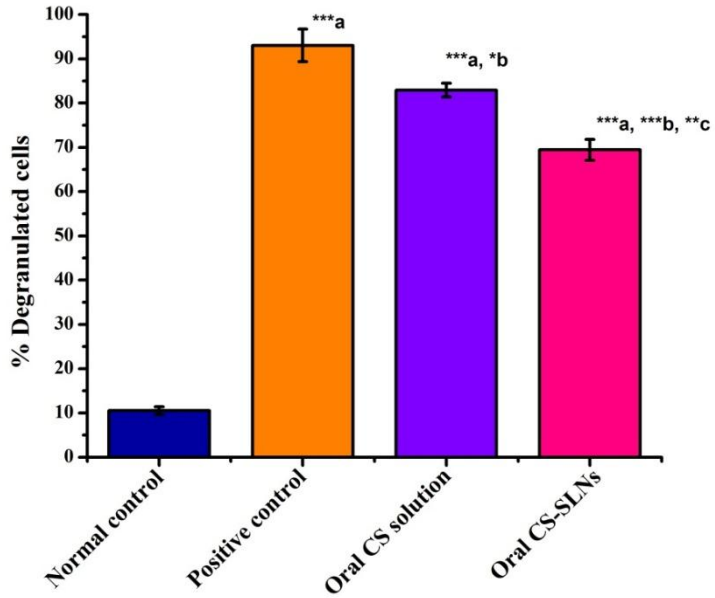

Figure 6.18 Effect of oral administration of CS solution and CS-SLNs on degranulation of peritoneal mast cells in rats (Dose: 20 mg/kg); Vertical bars represent ± SEM; n=6.

********p*<0.001, *****p*<0.01, ****p*<0.05; a *vs* normal control, b *vs* positive control and c *vs* oral CS solution; One-way ANOVA followed by Tukey's multiple comparison test**

In the normal control group, isolated peritoneal mast cells showed 10.515 ± 0.8813 % activation. Whereas, positive control group showed 93.033 ± 3.648 % activation of mast cells, upon incubation with compound 48/80. Prophylactic treatment with oral administration of the CS solution (20 mg/kg) and CS-SLNs (20 mg/kg) for 7 days in the rats has offered significantly higher (p<0.05) protection against mast cell degranulation and reduced the total number of activated mast cell. Oral administration of CS solution provided ~10.87 % protection against mast cell degranulation compared to positive control and showed 82.92 ± 1.558 % activation after incubation with compound 48/80. However, significantly much higher protection against mast cell degranulation was observed in case of CS-SLNs as compared to CS solution (p<0.001).

Table 6.16 Effect of oral administration of CS solution and CS-SLNs on compound 48/80 induced degranulation of peritoneal mast cells and histamine release in rats (Dose: 20 mg/kg)

Treatment Groups	% degranulated cells	Histamine release (µg/ml)
Normal Control	10.515 ± 0.881	0.033 ± 0.0019
Positive Control	93.033 ± 3.648***^{a}	0.190 ± 0.0083***^{a}
Oral CS solution	82.920 ± 1.558***^{a,}*^{b}	0.166 ± 0.0043***^{a,}*^{b}
Oral CS-SLNs	69.431 ± 2.380***^{a,}***^{b,}**^{c}	0.139 ± 0.0058***^{a,}***^{b,}*^{c}

*All values reported are mean ± SEM, (n=6). ***p<0.001, **p<0.01, *p<0.05; a vs normal control, b vs positive control and c vs oral CS solution; One-way ANOVA followed by Tukey's multiple comparison test.*

Oral administration of CS-SLNs provided ~25.36 % protection against mast cell degranulation compared to positive control and showed 69.431 ± 2.38 % activation after incubation with compound 48/80. Additionally, lower amount of histamine

release for CS-SLNs treated group compared to CS solution treated and positive control group suggested the better efficacy of CS-SLNs for stabilizing the mast cells from compound 48/80 like allergen evoked degranulation [199-202]. The enhanced efficacy for CS-SLNs compared to CS solution after oral administration indicated that CS-SLNs would have delivered significantly higher amount of CS in the systemic circulation by improving its GIT permeability and thereby, provided higher protection to the sensitized mast cells against degranulation, which in turn strengthens the findings of *in-vivo* pharmacokinetic study.

6.3 Summary

The present investigation provided an insight into the captivating aspects of SLNs by improving the pharmacokinetics and efficacy of CS after oral administration. The CS-SLNs were successfully engineered by double emulsification solvent evaporation method ($W_1/O/W_2$) with minor modifications. The Plackett-Burman screening design was employed for preliminary screening of large number of variables in order to identify critical variables affecting the formulation characteristics of CS-SLNs. A 3-level, 3-factor Box-Behnken experimental design was further used to optimize and to understand the combined influence of screened critical variables (i.e., concentration of lipid, concentration of surfactant and organic phase/aqueous phase ratio) on physicochemical properties of CS-SLNs, i.e., particle size, EE and PDI. The QbD approach suggested that the emphasis laid on the optimization process using Box-Behnken experimental design was enormously thorough with a high degree of prediction and realization, for optimization of the physicochemical properties of CS-SLNs. The optimized CS-SLNs showed particle size of 428 $\pm$ 4.6 nm, EE of 24.84 $\pm$ 0.56 % and PDI of 0.175 $\pm$ 0.048. The optimized batch has desirability of 0.636. The surface morphological and solid-state characterizations of optimized CS-SLNs

revealed the encapsulation of CS in an amorphous form without any interactions inside the spherical shaped SLNs. *In-vitro* release study of CS-SLNs in phosphate buffer pH 7.4 showed sustained release up to 24 hr by diffusion controlled process. CS-SLNs were found physically and chemically stable over the storage time period of 6 month without any significant change (p>0.05) in their physicochemical attributes, stored at room temperature (25 $\pm$ 2 ^{o}C) and refrigerated condition (4 $\pm$ 1 ^{o}C). *Ex-vivo* intestinal permeation study demonstrated ~2.96 fold improvements in CS permeation across the intestinal epithelial barrier by forming CS-SLNs as compared to pure CS solution. Further, *in-vivo* intestinal uptake study performed using confocal microscopy, after oral administration confirmed the permeation potential of CS-SLNs across intestinal barrier, as indicated by their strong green fluorescence. *In-vivo* pharmacokinetic study was performed in rats and revealed ~2.86 fold enhancements in oral bioavailability of CS after its encapsulation inside SLNs as compared to pure CS solution. Eventually, i*n-vivo* mast cell stabilizing activity performed in rats demonstrated significant protection against mast cell degranulation with oral administration of CS-SLNs than free CS solution. Conclusively, the developed CS-SLNs could definitely be considered as promising delivery strategy for favorably altering the existing marketed dosage form and dosing regimen of CS, with greater efficacy in various diseases.